JNeurosci
THE JOURNAL OF NEUROSCIENCE

Research Articles: Cellular/Molecular

Actin-binding protein cortactin promotes pathogenesis of experimental autoimmune encephalomyelitis by supporting leukocyte infiltration into the central nervous system

https://doi.org/10.1523/JNEUROSCI.1266-19.2019

Cite as: J. Neurosci 2020; 10.1523/JNEUROSCI.1266-19.2019

Received: 31 May 2019
Revised: 4 December 2019
Accepted: 19 December 2019

Actin-binding protein cortactin promotes pathogenesis of experimental autoimmune encephalomyelitis by supporting leukocyte infiltration into the central nervous system

Maryna Samus[1], Yu-Tung Li[1], Lydia Sorokin[2,3], Klemens Rottner[4] and Dietmar Vestweber[1,3,5]

[1]Max-Planck-Institute for Molecular Biomedicine, Münster, Germany
[2]Institute of Physiological Chemistry and Pathobiochemistry, [3]Cells-in-Motion Cluster of Excellence, University of Münster, Münster, Germany, [4] Helmholtz Center, Braunschweig, Germany

Abbreviated title: Cortactin supports leukocyte entry into the CNS

Number of pages: 29
Number of figures 9
Number of tables 0
Number of words: abstract: 237 ; introduction: 513 ; discussion: 1078

Conflict of interest: The authors declare no conflict of interest.

Acknowledgements: This work was supported in part by funds from the Max Planck Society (to D. Vestweber) and the Deutsche Forschungsgemeinschaft (SFB/TR128 to D. Vestweber).

[4]Correspondence:
vestweb@mpi-muenster.mpg.de
Dr. Dietmar Vestweber
Max-Planck-Institute for Molecular Biomedicine
Röntgenstr. 20
D 48149 Münster
Germany

Phone: + 49-251-70365-210
FAX: + 49-251-70365-299

Abstract

Leukocyte entry into the central nervous system (CNS) is essential for immune surveillance, but is also the basis for the development of pathologic inflammatory conditions within the CNS such as multiple sclerosis and its animal model, experimental autoimmune encephalomyelitis (EAE). The actin-binding protein, cortactin, in endothelial cells is an important player in regulating the interaction of immune cells with the vascular endothelium. Cortactin has been shown to control the integrity of the endothelial barrier and to support neutrophil transendothelial migration *in vitro* and *in vivo* in the skin. Here we employ cortactin gene inactivated (cortactin$^{-/-}$) male and female mice to study the role of this protein in EAE. Inducing EAE by immunization with a myelin oligodendrocyte glycoprotein peptide (MOG_{35-55}) revealed an ameliorated disease course in cortactin$^{-/-}$ female mice compared to WT mice. However, proliferation capacity and expression of IL-17A and IFNγ by cortactin-deficient and wildtype splenocytes did not differ, suggesting that the lack of cortactin does not affect induction of the immune response. Rather, cortactin deficiency caused decreased vascular permeability and reduced leukocyte infiltration into the brains and spinal cords of EAE mice. Accordingly, cortactin gene-deficient mice had smaller numbers of proinflammatory cuffs, less extensive demyelination and reduced expression levels of proinflammatory cytokines within the neural tissue compared to wildtype littermates. Thus, cortactin contributes to the development of neural inflammation by supporting leukocyte transmigration through the blood-brain barrier and, therefore, represents a potential candidate for targeting CNS autoimmunity.

Significance Statement

Multiple sclerosis (MS) is an autoimmune neuroinflammatory disorder, based on the entry of inflammatory leukocytes into the central nervous system (CNS) where these cells cause demyelination and neurodegeneration. Here, we use a mouse model for MS, experimental autoimmune encephalomyelitis (EAE), and show that gene inactivation of cortactin, an actin binding protein that modulates actin dynamics and branching, protects against neuroinflammation in EAE. Leukocyte infiltration into the CNS was inhibited in cortactin deficient mice and lack of cortactin in cultured primary brain endothelial cells inhibited leukocyte transmigration. Expression levels of proinflammatory cytokines in the CNS and induction of vascular permeability were reduced. We conclude that cortactin represents a novel potential target for the treatment of MS.

Introduction

Multiple sclerosis is an autoimmune neuroinflammatory disorder of the central nervous system (CNS), characterized by leukocyte-based demyelination and neurodegeneration. The entry of $CD4^+$ T cells and monocytes into the CNS are essential steps in the course of this disease and require diapedesis through the specialized endothelium of the blood-brain barrier (BBB). The barrier characteristics of this endothelium protect the CNS from changes in the milieu of the blood and require a higher level of contact integrity between endothelial junctions (Fenstermacher J, 1988; Sedlakova R, 1999). In addition, the endothelium of the BBB limits immune cell entry into the CNS and renders leukocyte diapedesis through this barrier a more demanding task (Sorokin, 2010; Ransohoff and Engelhardt, 2012).

Leukocyte extravasation is mediated by multiple adhesion molecules expressed by endothelial and immune cells and requires the support and dynamic reorganization of the actin cytoskeleton of both cell types (Nourshargh and Alon, 2014; Vestweber, 2015). Current knowledge about the role of endothelial actin-binding proteins in leukocyte adhesion and trans-endothelial migration is limited (Alon and van Buul, 2017), and only few studies have addressed their contribution to leukocyte extravasation at the BBB (Durieu-Trautmann et al., 1994; Li-ChunHsieh K, 2015).

In this study, we focus on cortactin, an actin-binding protein, which is involved in various cellular processes involving regulation of membrane dynamics and cell motility such as cell adhesion, migration, tumour invasion, and endocytosis (Cosen-Binker and Kapus, 2006; Schnoor et al., 2018). Cortactin is expressed in most cell types except leukocytes which express the related protein Hematopoietic cell-specific lyn substrate 1(HS1) (van Rossum AG, 2005). One of the major molecular functions of cortactin is to bind and activate the actin-filament nucleation complex Arp2/3(Uruno T, 2001), which facilitates the branching of F-actin (Mullins RD, 1998).

The role of cortactin in the regulation of the endothelial barrier properties, actomyosin contractility, and leukocyte transendothelial migration (diapedesis) was shown *in vitro* (Dudek et al., 2004; Jacobson et al., 2006; Yang et al., 2006b; García Ponce A, 2016) and in a cytokine-induced

inflammation model in the cremaster muscle (Schnoor et al., 2011). Cortactin-deficient animals have increased basal vascular permeability in the skin, and show enhanced sensitivity to permeability-inducing inflammatory mediators such as histamine; however, neutrophil transmigration is reduced (Schnoor et al., 2011). In accordance with these data, *in vitro* cortactin, together with F-actin and ICAM-1, surround transmigrating polymorphonuclear leukocytes and facilitate their adhesion and subsequent extravasation through HUVEC monolayers (Yang et al., 2006b).

Here, we have analyzed the potential relevance of cortactin in the endothelial barrier function of the BBB and for the development of the clinical symptoms of EAE. We found that cortactin gene inactivation reduced entry of $CD4^+$ T cells and myeloid cells into the brain and spinal cord parenchyma, and at the same time, vascular permeability induction in the inflamed CNS was reduced. These protective effects decreased inflammation and demyelination within the CNS and significantly lowered EAE clinical symptoms. This implicates cortactin as an important player in leukocyte recruitment to the CNS and suggests that it may represent a potential target in the treatment of autoimmune neuroinflammatory diseases, like multiple sclerosis.

Material and Methods

Mice

Cortactin-deficient mice (hereafter referred to as Cttn$^{-/-}$) were generated as previously described (Schnoor et al., 2011). For controls, age- and gender-matched littermates or C57Bl/6 mice were used. Experiments for Fig. 1 were performed only with female mice, while other experiments were done with mice of both sexes. All experiments were conducted according to German animal welfare guidelines and were approved by the Landesamt fuer Natur, Umwelt und Verbraucherschutz Nordrhein-Westfalen.

Antibodies

The following primary antibodies were used: anti-cortactin (clone 4F11, Millipore), anti-claudin-5-Alexa Fluor 488 (clone 4C3C2, Invitrogen), anti-occludin (ab31721, Abcam), anti-VE-cadherin (VE42)(Broermann et al., 2011), anti-ZO-1 (40-2200, Invitrogen), rabbit serum against pan-laminin(Sixt et al., 2001), rat anti-CD45, FITC-conjugated rat anti-CD4, anti-CD4-BV421 (#100544), FITC-conjugated rat anti-CD8, FITC-conjugated rat anti-Ly6G, FITC-conjugated rat anti-CD11b, APC-conjugated rat anti-CD45, anti-T-bet (#644804), anti-RORγt (#12-6988-82, Invitrogen), anti-IL-17A (#506910), IFN-γ (#505826), anti-ICAM1 (YNI-1.1). FITC-conjugated rat anti-IgG2a and -rat anti-IgG2b, APC-conjugated rat anti-IgG2 and rabbit anti-FcγRII+III (2.4G2, hybridoma provided by Prof. Alf Hamann). All primary antibodies, if not stated otherwise, were purchased from BD Pharmingen. The following secondary antibodies were used: Alexa Fluor-488 donkey anti-rabbit, Alexa Fluor-488 donkey anti-mouse, Alexa Fluor-647 donkey anti-rat. All secondary antibodies were purchased from Invitrogen.

Induction of active EAE

For induction of active EAE, 8–11-week-old mice were used. For controls, age- and gender-matched littermates or C57BL/6 mice were used. On day 0, mice were immunized subcutaneously with 20 µg MOG_{35-55} peptide (Sigma Aldrich) per mouse emulsified in complete Freund´s adjuvant containing M. tuberculosis H37RA (Difco Laboratories). Pertussis toxin (200 ng) (Sigma Aldrich) was injected intraperitoneally on day 0 and day 2. Mice were observed daily for up to 30 days after immunization. The clinical scores were assigned based on the following criteria: (0) no signs of disease; (0.5) loss of the tail tone or abnormal gate; (1) flaccid tail and absence of curling at the tip when picked up; (1.5) completely flaccid tail and mild hindlimb weakness; (2) hindlimbs are severely weak, mouse is able to move in a waddling gait; (2.5) hindlimbs are partially paralyzed with some movement observed; (3) hindlimbs and lower back are completely paralyzed; (3.5) hindlimbs and lower back are completely paralyzed, weakness in the forelimbs; (4) forelimbs are additionally paralyzed, mouse cannot move; (5) death. Dead mice were not included in clinical score measurements. Mice were supplied with Diet Gel ® Recovery (Clear H2O), serving as both a food and liquid source. To reduce suffering, mice reaching stage 4 were sacrificed.

Fluorescence-activated cell sorting (FACS)

Cells from lymph nodes and spleens were isolated by sieving through 70 µm cell strainers and the single cell suspensions were kept on ice-cold PBS. Peripheral blood was collected by cardiocentesis. Erythrocytes were lysed with ACK lysis buffer (Thermo Fisher Scientific) for 3 min at RT. For a collection of immune cells from the brain and the spinal cord, mice were perfused with ice-cold PBS prior to tissue removal; cells were collected by sieving through 100 µm cell strainers, followed by separation into neuronal and leukocyte populations by discontinuous density gradient centrifugation using isotonic Percoll (Amersham). The leukocyte total number was counted (CASY, Schärfe-System). For relative quantification of leukocyte subtypes, mouse Fc-receptors were blocked with anti-FcγRII+III and cells were stained with the cell-specific antibodies. To distinguish between CD11b+ infiltrated cells and microglia from the brain, we gated on the CD45high and CD45low populations,

176 respectively. Flow cytometry was performed with the FACSCanto™ II (Becton Dickinson) and data
177 evaluated with FlowJo 7.2.5. For flow cytometric analysis of T cell cytokine expression, splenocytes
178 and leukocytes from brain and spinal cord were isolated from mice at the peak of EAE. Cells were
179 stimulated for 4h at 37°C with 500 ng/ml PMA and 1 µg/ml ionomycin in the presence of 5 µg/ml
180 protein transport blocker Brefeldin A. After stimulation, cells were stained with anti-CD4-BV421
181 followed by fixation and permeabilization (eBioscience™ Foxp3/Transcription Factor Staining Buffer
182 Set) according to the manufacturer's instructions. Transcription factors T-bet and RORγt, and
183 intracellular cytokines IL-17A and IFN-γ were stained. Cells were acquired using FACS CytoFlex S
184 (Beckman Coulter) and data were analyzed with FlowJo 7.2.5.
185
186 ***In vitro* cell proliferation assay**
187 For assessment of cell proliferation, WT and cortactin-deficient mice were immunized with MOG_{35-55}
188 as described above. At day 10 post-immunisation (p.i.), mice were sacrificed and spleens were
189 removed. Single-cell suspensions were obtained by sieving the spleens through the 40 µm strainer.
190 Cells were cultured in 96-well plates at $1x10^5$ cells/well in RPMI 1640 medium, supplemented with
191 10% heat-inactivated fetal bovine serum, 2 mM L-glutamine, 100 U/mL penicillin-streptomycin, 1%
192 non-essential amino acids, 1mM sodium pyruvate and 0.5 mM β-mercaptoethanol. Splenocytes were
193 incubated for 72 h after isolation in the absence or presence of MOG_{35-55} (0.5, 1 and 5 µg/ml). Cell
194 proliferation assays were performed using a BrdU cell proliferation kit (Merck) according to the
195 manufacturer's instructions. BrdU reagent was added for the final 24 h. Incorporation of BrdU reagent
196 was measured on a Synergy2 microplate reader (BioTek) at a wavelength of 450 nm. All experiments
197 were performed in triplicate.
198
199 **Determination of mRNA expression levels using quantitative Real-Time RT-PCR**
200 Mice were sacrificed at peak EAE and perfused with ice-cold PBS. Total RNA from the brains and the
201 spinal cords was extracted using Trizol (Invitrogen). RT-PCR was carried out using SuperScript II

Reverse Transcriptase kit (Invitrogen) according to the manufacturer's instructions in a reaction volume of 20 µl. cDNA samples were subjected to qRT-PCR using iTaq Universal SYBR Green Supermix (Bio-Rad) and amplification was performed using 7300 Real Time PCR System (Applied Biosystems). For qRT-PCR amplification of cDNA, the following primers (Sigma Aldrich) were used: CCR2-FW: ATTCTCCACACCCTGTTTCG and CCR2-RE: CTGCATGGCCTGGTCTAAGT; CXCL1-FW: GTTCCAGCACTCCAGACTCC and CXCL1-RE: TGGGGACACCTTTTAGCATC; GAPDH-FW: GCCACCCAGAAGACTGTGGAT and GAPDH-RE: GGGATGACCTTGCCCACAG; IFNγ-FW: CTGGAGGAACTGGCAAAAGG and IFNγ-RE: CTGGACCTGTGGGTTGTTGA; IL-1β-FW: ATCCCAAGCAATACCCAAAG and IL-1β-RE: GTGCTGATGTACCAGTTGGG; IL-6-FW: CCTTCCTACCCCAATTTCCAAT and IL-6-RE: AACGCACTAGGTTTGCCGAGTA; IL-17A-FW: CGCAAAAGTGAGCTCCAGA and IL-17A-RE: TGAGCTTCCCAGATCACAGA; MCP-1-FW: GCATCTGCCCTAAGGTCTTC and MCP-1-RE AAGTGCTTGAGGTGGTTGTG; RANTES-FW: TCTTGCAGTCGTGTTTGTCA and RANTES-RE: CAGGGAAGCGTATACAGGGT; TNFα-FW: AGCCCCCAGTCTGTATCCTTCT and TNFα-RE: AAGCCCATTTGAGTCCTTGATG; VE-cad-FW: TCCTCTGCATCCTCACTATCACA and VE-cad-RE: GTAAGTGACCAACTGCTCGTGAAT; Claudin-5-FW: GTGGAACGCTCAGATTTCAT and Claudin-5-RE: TGGACATTAAGGCAGCATCT; Occludin-FW: AGACCCAAGAGCAGCCAAAG and Occludin-RE: GGAAGCGATGAAGCAGAAGG; ZO-1-FW: CCACCTCTGTCCAGCTCTTC and ZO-1-RE: CACCGGAGTGATGGTTTTCT. The cycling conditions were as recommended by the manufacturer: enzyme activation at 50°C for 2 min, initial denaturation at 95°C for 10 min, followed by 40 cycles of denaturation at 95°C for 15 s and annealing/elongation at 60°C for 1 min. Gene expression was normalized to GAPDH and analyzed using the ΔΔCt method. Results were expressed relative to those obtained with WT samples.

In vitro static transmigration assay

A total of 4 x 10^4 MBMEC cells/well of 3-µm transwells (Corning Life Sciences), coated with 40% gelatin and 0.1 mg/ml fibronectin (Sigma Aldrich) were grown for 4-5 days and stimulated 16 hours before the assay with 5nM TNFα (Peprotech). OTII-OVA T cells were stimulated for 2 days with 1.5% IL-2 and added 3 x 10^4 cells/transwell on top of MBMECs. The lower compartments of the transwell chambers were filled with transmigration media, containing SDF-1 (100 ng/ml) as a chemoattractant. After 1 h and 3.5 h cells from the lower compartment of the transwell chamber were harvested and counted using CASY (Schärfe-System).

In vitro static adhesion assay

A total of 4 x 10^4 MBMEC cells/well of gelatin-fibronectin coated 96-well plate were grown for 4-5 days and stimulated 16 hours before the assay with 5 nM TNFα. OTII-OVA T cells were stimulated for 2 days with 1.5% IL-2, labeled with 2 µM Cell Tracker Green CMFDA (Invitrogen ^{TM}) and added 1 x 10^5 cells/well on top of MBMECs for 30 min. Next, wells were washed 5 times with PBS containing 1 mM each of $CaCl_2$ and $MgCl_2$, fixed with 4% PFA and analyzed under an inverted epifluorescent microscope Zeiss Axiovert 200m. The results were quantified with ImageJ 1.48v.

In vitro adhesion assay under flow

A total of 8 x 10^4 MBMEC cells/channel, of the six-channel µ-Slide $VI^{0.4}$ (Ibidi) coated with gelatin and fibronectin (as above), were grown for 3-4 days and stimulated 16 hours before the assay with 5nM TNFα. OTII-OVA T cells were stimulated for 2 days with 1.5% IL-2 and labeled with 2 µM Cell Tracker Green CMFDA. Labeled T cells were resuspended at 2.5 x 10^5/ml (20 ml per flow) in HBSS with 1mM each of $CaCl_2$/$MgCl_2$ 1.2% BSA and 25mM HEPES, mixed with SDF1 (50 ng/ml) and added to the MBMEC monolayer at 0 to 2 dyn/cm2 in 20 min. Videos were recorded under a 10x objective and analyzed with TrackMate 20.

Immunohistochemistry

The brains were isolated at peak EAE (post-immunization day 17-20), embedded in O.C.T Compound (Tissue-Tek), snap-frozen, and sectioned on a cryotome from dorsal to ventral. For staining, six-micrometer sections from 4 different regions were taken. Sections were air-dried for 30 min, fixed for 15 min with cold methanol at –20◦C, washed twice with PBS, and blocked with 1% BSA/10% goat serum in PBS for 1 h. Incubation with primary anti-pan-laminin and anti-CD45 antibodies was performed over night (O/N) at 4°C. Bound antibodies were visualized using Alexa Fluor 488-conjugated donkey anti-rabbit and Alexa Fluor 568-conjugated donkey anti-rat secondary antibodies, which were applied for 1 h. Sections were mounted with Dako Fluorescence Mounting Medium and the number of inflammatory cuffs/section was counted using a Zeiss Axioscope 2.

For brain vessel staining, the brains were isolated, fixed for 4 h with 4% paraformaldehyde (PFA) at 4◦C, embedded in 4% low melting agarose and stored at 4°C. Thick sections of 100 µm were cut on a vibratome, permeabilized with 0.3% Triton X-100/0.1% Tween20 in PBS for 1 h at 4°C and blocked with 4% BSA/0.3% Triton X-100 in PBS for 1 h at 4°C. Subsequent incubation with primary and secondary antibodies (Alexa Fluor 488-conjugated donkey anti-rabbit) was performed O/N at 4°C. Slides were mounted with Dako Fluorescence Mounting Medium and examined with a confocal microscope, Zeiss LSM 880, and analysed using ImageJ 1.48v.

Spinal Cord Histological Analysis

For evaluation of immune-mediated inflammation in the spinal cord, spinal cords were fixed in 4% PFA for 2 days at 4°C, re-hydrated in 15% and 30% glucose for 3 days each, snap-frozen in O.C.T Compound, and sectioned on a cryotome. Ten-micrometer sections from the lower lumbar part of the spinal cord were stained for Hematoxylin & Eosin and Luxol Fast Blue (LFB) (Solvent blue 38, Sigma Aldrich) to evaluate the number of inflammatory foci and the degree of demyelination, respectively. Sections were analyzed with an inverted epifluorescent microscope, Zeiss Axiovert 200, and data quantified with ImageJ 1.48v.

BBB permeability *in vivo*

For analysis of BBB permeability during EAE development, 100 µl of 2% Evans blue in PBS was injected intravenously into the tail vein; mice were perfused with PBS 1h or 24 h after injection, and brains and spinal cords were removed. Tissues were placed in formamide for 5 d, and the concentration of Evans blue was measured at 620 nm (Shimadzu). Kidney tissue from naïve mice treated in the same manner served as positive controls. The amount of tracer in the tissues was determined from the formula A620/wet weight (g).

Isolation of mouse brain microvascular endothelial cells (MBMEC)

MBMEC were obtained as described previously (Ruck T, 2014). Briefly, brains from 4-5 mice (10-14 -week-old) were isolated. The forebrains, without meninges, were transferred to a tube with13.5 ml DMEM. The tissue was minced first with a plastic 25 ml pipette and then using a 10 ml pipette. The suspension was further digested with 0.6 ml 10 mg/ml collagenase and 20 µl 10 mg/ml DNAse in DMEM for 1 h at 37°C. Then 10 ml DMEM was added and cells were centrifuged at 1400 rpm for 20 min at 4°C. To remove the myelin, the pellet was resuspended in 25 ml 20% BSA-DMEM and centrifuged at 1500 rpm for 30 min at 4°C. The pellet was resuspended in 10 ml DMEM and further digested with 0.3 ml collagenase (10 mg/ml in DMEM), 0.3 ml dispase (10U/ml) and 10 µl DNAse for 1 h at 37°C. 10 ml DMEM was then added and the cells were centrifuged at 1400 rpm for 20 min at 4°C. The cells were resuspended in 2 ml endothelial cell media and seeded onto 12-well plates, coated with 40% gelatin and 0.1 mg/ml fibronectin (Sigma Aldrich).

Immunocytochemistry

For staining, a total of 5 x 10^4 MBMEC /well of gelatin-fibronectin coated (as above), 8-well chamber slides (Ibidi) were grown for 4-5 days. Cells were washed twice with PBS, permeabilized with 0.5% Tween-20 for 10 min and fixed with 4% PFA for 5 min at RT. Non-specific binding was blocked with 3%BSA/PBS, pH 7.4, for 1 h at RT. Subsequently, cells were incubated for O/N at 4°C with anti-

cortactin, anti-occludin, anti-VE-cadherin, anti-ZO-1 or anti-ICAM-1 primary antibodies diluted in PBS containing 2% BSA, followed by incubation with fluorescently-conjugated secondary antibodies (Invitrogen). The cells were washed twice with PBS, stained with 2 µg/ml Hoechst 33342 (Invitrogen) for 5 min and kept in 0.01% NaN_3/PBS. Staining was analyzed a confocal microscope, Zeiss LSM 880, and data analysed with ImageJ 1.48v processing software.

Experimental design and statistical analysis

Mice were male or female, and the experimental groups were gender- and age-matched. For all experiments, the number of mice used and the number of independent experiments is stated in the figure legends. All data values are presented as the mean ± standard error of the mean (SEM). Statistical analysis was performed using GraphPad Prism 6. Distribution of data was evaluated for normality using D'Agostino & Pearson omnibus test. The significance between two groups was evaluated using the unpaired Student´s *t* test or by Mann-Whitney Rank Sum Test. Comparison between more than two groups was analyzed using one-way or two-way ANOVA followed by Tukey *post hoc* test. ANOVA analysis presented as $F_{(x, y)}$, where x is degree of freedom from between the sample groups and y is degree of freedom from within the samples. P-values are indicated by asterisks: * = $p \leq 0.05$; ** = $p \leq 0.01$; *** = $p \leq 0.001$; **** = $p \leq 0.0001$; ns = not significant.

Results

Cortactin deficiency results in reduced EAE severity

To examine the role of cortactin in neuroinflammation and leukocyte extravasation across the blood brain barrier (BBB) we analyzed the development of active EAE in cortactin gene inactivated ($Cttn^{-/-}$) mice. To this end, we induced active EAE in $Cttn^{-/-}$ and WT littermates by immunization with the MOG_{35-55} peptide. EAE clinical symptoms developed in the form of gradual paralysis, peaking between day 16 and 20 post immunization (Fig. 1A). Evaluation of the clinical symptoms showed that the overall severity of disease in $Cttn^{-/-}$ mice was significantly lower than in WT mice (Fig. 1A–C), with no difference in the day of disease onset (Fig. D). The percentage of mice with severe clinical scores was 3 times higher among WT mice (84.2%) compared to cortactin-deficient animals (26.3%), and the majority of the knockout mice (57.9%) developed mild clinical symptoms, compared to 15.8% of WT mice (Fig. 1E). Taken together, these data demonstrate that the absence of cortactin results in reduced EAE severity.

Immune response to MOG_{35-55} peptide is not affected by lack of cortactin

When bred under pathogen-free conditions, healthy $Cttn^{-/-}$ mice developed normal without any visual defects and had normal peripheral leukocyte, platelet and erythrocyte counts similar to control animals (Schnoor et al., 2011). Since EAE commences with induction of an peripheral immune response, we tested whether cortactin gene inactivation could affect this process. To this end, we analyzed the proportions and numbers of $CD4^+$ T cells and $CD11b^+$ macrophages in the blood, lymph nodes and spleens of $Cttn^{-/-}$ and WT animals before EAE onset (day 10 p.i) (Fig. 2A) and at the peak disease (Fig. 2B), revealing no differences between $Cttn^{-/-}$ and WT animals.

As another approach to test a potential role of cortactin in peripheral immune responses, we performed *in vitro* BrdU colorimetric proliferation assays to compare the proliferation of WT and $Cttn^{-/-}$ splenocytes, isolated on day 10 post immunization and restimulated *in vitro* with different

concentrations of MOG_{35-55} peptide. A larger proportion of splenocytes in both WT and $Cttn^{-/-}$ EAE mice showed active proliferation compared to healthy animals (non-EAE), indicating the efficiency of *in vivo* splenocyte priming towards the myelin antigen. *In vitro* restimulation with MOG_{35-55} peptide further increased rthe proportion of proliferating splenocytes in EAE animals. In all conditions, we could not detect differences in splenocyte proliferation of WT and $Cttn^{-/-}$ mice (Fig. 2C), consistent with our *in vivo* data. Lastly, we detected no differences in IL-17A and IFNγ expression by MOG-reactivated splenocytes (Fig. 2D). Taken together, the absence of cortactin does not interfere with the induction of the immune response.

Cortactin deficiency restricts leukocyte infiltration and inflammation in the CNS

To test whether a decrease in EAE scores in the absence of cortactin was caused by reduced leukocyte recruitment into the brain parenchyma, we isolated immune cells from the brain of WT and $Cttn^{-/-}$ mice at a time point when WT mice reached the peak clinical score of EAE. The total number of isolated leukocytes was determined by a cell counter and subsequently quantified by flow cytometry for the presence of $CD45^{high}$ leukocytes, $CD4^+$ T cells, $CD8^+$ T cells, $CD11b^+$ macrophages, and Ly6G neutrophils. Our results showed that cortactin deficiency resulted in a significant 45% decrease in the proportion of $CD45^{high}$ immune cells (Fig. 3A) and in the different leukocyte populations that had infiltrated into the inflamed brains: $CD4^+$ T cells (49% reduced), $CD8^+$ T cells (50% reduced), $CD11b^+$ macrophages (33% reduced), and Ly6G neutrophils (44% reduced) (Fig. 3B, C, D, and E). At the same time, there was no difference in the numbers of $CD11b^+CD45^{low}$ microglia in knockout and WT brains (Fig. 3F). Similar results were obtained for the spinal cord, with a decrease in $CD45^{high}$ cells (46% reduced), $CD4^+$ T cells (50% reduced) and $CD11b^+$ macrophages (40% reduced) in $Cttn^{-/-}$ compared to WT mice (Fig. 3G, H, I). A more detailed analysis of CD4 T cell subsets revealed that at peak of disease, cortactin deficiency caused a strong reduction of Th17 cells, but not Th1 cells, in spinal cord (Fig. 3K) whereas no changes were found for both T cell subtypes in brain (Fig. 3J) and spleen (Fig. 3L).

As an additional criterion for the efficiency of leukocyte infiltration into the CNS, we used immunohistochemistry to analyze the presence of inflammatory cuffs in the brains of Cttn$^{-/-}$ and WT mice. Inflammatory cuffs are typical structures that are observed in EAE, formed due to the accumulation of immune cells between endothelial and parenchymal basement membranes of the BBB (Sixt et al., 2001). These structures were visualized at the peak of EAE by staining for the two basement membranes using pan-laminin antibody and with anti- CD45 to mark leukocytes (Fig. 3M). The number of cuffs were counted in 4 different brain sections (cutting intervals 240 μm) per animal and the average number of cuffs per section was calculated. Quantification showed a significant 48% decrease in the number of proinflammatory cuffs in Cttn$^{-/-}$ mice compared to their WT counterparts (Fig. 3N). The average size of cuffs was unaffected by cortactin gene deficiency (Fig. 3O).

To evaluate the degree of inflammation in the spinal cord at peak EAE, we performed H&E and LFB staining of frozen, transverse sections taken from the spinal cord lumbar region to visualise leukocyte infiltration and neurodegeneration (demyelination), respectively. The severity of leukocyte infiltration was quantified by determining the average number of inflammatory foci per section, using 4 sections per mouse. As shown in Fig. 4A and B, cortactin-deficient animals had a significant reduction in the number of inflammatory foci compared to WT mice. Neurodegeneration in the spinal cord was assessed by LFB staining, were absence of staining defines sites of demyelination, and quantified as average demyelinated area per section from 3 different sections per animal; data was expressed relative to the demyelination observed in WT mice. This revealed that Cttn$^{-/-}$ mice exhibited 51% less myelin loss than WT animals (Fig. 4A and C). These data collectively suggest that cortactin is important for the process of immune cell diapedesis into the CNS, thereby, supporting the progression of pathological changes and the development of neuroinflammation during EAE.

Cortactin-deficient mice showed reduced expression of proinflammatory cytokines

We next tested whether the absence of cortactin affected expression of proinflammatory mediators in the inflamed CNS. To this end, we isolated RNA from the brains and spinal cords of WT and Cttn$^{-/-}$

mice at peak EAE and performed quantitative RT-PCR. Several proinflammatory cytokines, chemokines, and chemokine receptors were analysed, revealing generally lower levels of production of proinflammatory mediators in the brains of Cttn$^{-/-}$ mice compared to WT mice (Fig. 5). The most profound difference was observed for RANTES, a chemokine for T cells and monocytes. A significant decrease in TNFα and CCR2, but not IFNγ, IL-1β, IL-6, IL-17A, MCP-1 and CXCL1, expression was measured in Cttn$^{-/-}$ compared to WT brains. In the inflamed spinal cord, most analyzed cytokines and chemokine receptors analysed were expressed at significantly lower levels in Cttn$^{-/-}$ mice compared to WT mice, including TNFα, IFNγ, IL-1β, IL-6, CCR2, RANTES, MCP-1 and CXCL1 (Fig. 5). IL-17A was also reduced, but not at a statistically significant level. The reduced levels of proinflammatory cytokines in the absence of cortactin is consistent with the decreased leukocyte infiltration observed in these mice and probably contributes to the lower EAE scores in cortactin-deficient animals.

Cortactin-deficient mice have reduced vascular permeability in the CNS

We previously showed that cortactin gene inactivation causes a significant increase in the basal and histamine-induced vascular permeability in the skin (Schnoor et al., 2011). We therefore tested whether the absence of cortactin has similar effects on vascular permeability in the CNS during EAE. EAE-subjected WT and Cttn$^{-/-}$ mice were injected at day 10 i.p. with Evans blue and leakage into tissues was measured 24 h later; non-immunized, healthy WT and Cttn$^{-/-}$ mice served as controls. In general, increased vascular permeability was measured in the brain and spinal cords of WT EAE mice compared to healthy WT and Cttn$^{-/-}$ controls (Fig. 6A, B). However, as shown in Fig. 6B, healthy Cttn$^{-/-}$ mice showed an increase in the basal permeability of blood vessels in the spinal cord, consistent with our previous data from the skin, and little or no increase in permeability during EAE. Comparison of the MOG-injected animals revealed significant 30% and 58% reductions in Evans blue leakage into the brain (Fig. 6A) and the spinal cord (Fig. 6B) of knockout mice compared to WT. Vascular permeability in the kidney of the same mice, which served as control, was not affected by cortactin gene inactivation (Fig. 6C). Similar experiments were performed at peak of clinical score, with Evans Blue being

injected for only 1 h before measuring leakage. We detected a significant reduction in permeability in the spinal cord of Cttn$^{-/-}$ mice (Fig. 6E), whereas different from the onset of EAE, brain permeability at the peak of disease was similar in WT and Cttn$^{-/-}$ mice (Fig. 6D). Vessel density in the brain was similar in WT and Cttn$^{-/-}$ mice (Fig. 6F and G). Collectively, our results suggest that cortactin gene inactivation protects from an increase in vascular permeability in EAE, most likely due to reduced entry of inflammatory cells.

Cortactin supports diapedesis of T cells through mouse primary brain endothelial cells

Due to the special barrier function of the BBB endothelium, we analyzed the migration of CD4^{+} T cells across monolayers of primary MBMEC in *in vitro* transmigration assays. First, we confirmed expression of cortactin in WT MBMECs, which was absent in the MBMECs from Cttn$^{-/-}$ mice (Fig. 7). Cortactin was found close to junctions but also throughout the cell. It has been previously reported that silencing of cortactin by shRNA in human brain microvascular endothelial cells leads to fragmented staining of claudin-5, occludin and ZO-1 (Stamatovic SM, 2015). However, comparison of occludin, VE-cadherin and ZO-1 staining patterns in of WT and Cttn$^{-/-}$ primary MBMECs revealed no differences. Likewise, whole mount staining of blood vessels in vibratome sections of mouse brains from WT and Cttn$^{-/-}$ mice showed no differences in the junctional expression patterns of claudin-5, VE-cadherin and ZO-1 (Fig. 8). Analyzing gene expression of claudin-5, VE-cadherin and ZO-1 by qRT-PCR in brain and spinal cord of mice with EAE at the peak of disease and of WT mice revealed no gross changes between the two genotypes either, with the exception of a slight reduction of VE-cadherin levels in the brain of healthy (but not diseased) Cttn$^{-/-}$ mice and a slight increase of occludin expression in the spinal cord of diseased (but not healthy) Cttn$^{-/-}$ mice (Fig. 9).

We next tested whether the absence of cortactin affects the diapedesis of T cells through primary MBMEC monolayers. We found that transmigration through Cttn$^{-/-}$ brain endothelial cells was indeed reduced compared to WT endothelial cells (Fig. 10A). Interestingly, adhesion of T cells to MBMEC under static conditions was similar for both genotypes (Fig. 10B). However, under flow

conditions T cell adhesion to MBMEC was reduced in the absence of cortactin (Fig. 10C). We conclude that cortactin in mouse brain endothelial cells supports the docking and transmigration of $CD4^+$ T cells. Quantifying the expression level of ICAM-1 on primary MBMEC from $Cttn^{-/-}$ and WT mice showed very weak expression in the absence of cytokines, which was strongly upregulated by TNF-α to similar levels for both genotypes (Fig. 11). Thus, the expression level of ICAM-1 is not affected by cortactin.

Discussion

Leukocyte extravasation through the BBB is a crucial step in the development of autoimmune demyelinating conditions of the CNS such as multiple sclerosis and the respective animal model EAE. Yet, in contrast to the endothelium of other organs the endothelium of the BBB represents a special barrier that is less easily overcome by solutes and leukocytes. Mechanistic details about the transmigration of leukocytes through the BBB are less well understood than for the endothelium in other tissues. Here, we show that the actin-binding protein cortactin is required for immune cell infiltration into the CNS in the context of EAE. EAE severity was clearly reduced in cortactin gene inactivated mice. Accordingly, pro-inflammatory cytokine levels in the CNS were reduced and inflammation-induced vascular permeability was attenuated. Since we could rule out a negative effect of the lack of cortactin on the induction of the immune response, we conclude that interference with endothelial cortactin inhibits the entry of inflammatory cells into the CNS, which was further substantiated by less efficient migration of $CD4^+$ T cells through primary brain endothelial cells isolated from cortactin$^{-/-}$ mice.

The reduced leukocyte transmigration efficiency across the BBB of Cttn$^{-/-}$ mice is reminiscent of our findings with cortactin deficient primary lung endothelial cells (Schnoor et al., 2011) and shows that, despite the special character of brain endothelial cells, the contribution of cortactin to the transmigration process is of basic importance and relevant in both endothelial cell subtypes. In our previous study, we found that cortactin was required for the clustering of endothelial ICAM-1 around adhering/transmigrating neutrophils at the diapedesis pore, which was dependent on ICAM-1-triggered RhoG activation (Schnoor et al., 2011). Cortactin acted upstream of the activation of RhoG in this process. This is in accordance with other studies demonstrating tyrosine phosphorylation of cortactin upon crosslinking of ICAM-1 (Durieu-Trautmann et al., 1994) and resulting coprecipitation of cortactin with ICAM-1 (Tilghman and Hoover, 2002). In line with this, silencing of cortactin in cultured endothelial cells inhibits accumulation of ICAM-1 at sites of neutrophil attachment and inhibits

transmigration(Yang et al., 2006b; Yang et al., 2006a). The latter study suggested that silencing of cortactin does not impair adhesion of neutrophils to EC in assays under static conditions. However, *in vivo*, we have shown that neutrophil adhesion and extravasation is reduced in postcapillary venules of the cremaster in the absence of cortactin, arguing that cortactin-dependent ICAM-1 clustering might be needed for neutrophil arrest as well as for the transmigration process under physiological flow conditions (Schnoor et al., 2011). Since ICAM-1 is also an important player for the entry of leukocytes into the CNS (Lyck and Engelhardt, 2012) it may be that cortactin-dependent clustering of ICAM-1 is also needed in postcapillary venules of the brain for leukocyte extravasation.

In vivo evidence for the relevance of cortactin for leukocyte extravasation was so far limited to neutrophils. Our flow cytometry analyses in the present study revealed a decrease in all measured leukocyte types that had infiltrated into the brain of $Cttn^{-/-}$ mice, including $CD4^+$ and $CD8^+$ T cells, macrophages and neutrophils. We conclude therefore that cortactin contributes to basic mechanisms of the transmigration process, which are common to a large repertoire of leukocyte types.

Of interest, we detected in $Cttn^{-/-}$ mice a selective inhibition of Th17 lymphocyte recruitment to spinal cord, whereas Th1 cell recruitment was like in WT mice. Considering that caveolar transcytosis was reported to be required for Th1, but not Th17, cell entry into the CNS (Lutz et al., 2017), our results may suggest that cortactin is needed for a junction-related extravasation route, that may be more relevant for Th17 cells. This may warrant future studies to elucidate a possible role of cortactin in the paracellular diapedesis of leukocytes.

We have previously shown that cortactin contributes to vascular integrity, since cortactin deficiency led to increased basal vascular permeability in the skin and the permeability-enhancing effect of histamine was substantially increased in cortactin gene inactivated mice compared to WT mice (Schnoor et al., 2011). In agreement with these results, we show here that the absence of cortactin caused increased basal vascular permeability in the spinal cord blood vessels. By contrast, we found no such effect in the brain or in the kidney, highlighting the fact that regulatory elements determining baseline junctional integrity varies between vascular beds of different organs. Despite the junction

521 stabilizing function of cortactin, the lack of cortactin protected from vascular leak formation in brain
522 and spinal cord during EAE. This is probably due to the fact that cerebral permeability tightly follows
523 leukocyte extravasation (Leibowitz S, 1972; Butter C, 1991). Transmigration of immune cells through
524 the BBB contributes to an increase in vascular permeability in a number of ways - by upregulation of
525 the production and secretion of proinflammatory cytokines, changes in factors such as matrix
526 metalloproteinase activity, reactive oxygen species, histamine and neurotrophins. These factors
527 contribute to the disruption of the molecular organization of the BBB and increases in the expression of
528 adhesion molecules and chemoattractants by the brain microvascular endothelial cells, thereby,
529 perpetuating the infiltration of immune cells into the CNS (Larochelle C, 2011). In accordance with
530 this hypothesis, we found reduced levels of pro-inflammatory cytokines in brains and spinal cords of
531 cortactin$^{-/-}$ mice. Therefore, we suggest that the decrease in vascular permeability observed in cortactin
532 deficient mice during EAE is due to the reduced infiltration of immune cells into the CNS and the
533 resulting lower levels of BBB disrupting pro-inflammatory mediators. This positive correlation
534 between the transmigration of leukocytes and the induction of permeability on the tissue level should
535 not be mistaken with a direct effect of the diapedesis process on junctional leakiness. It is now well
536 documented that the diapedesis process does not *per se* cause enhanced leakiness (Cutler RW, 1967;
537 Leibowitz S, 1972; Baluk et al., 1998; Schnoor et al., 2011; Wessel et al., 2014; Heemskerk et al.,
538 2016). The supportive effect of cortactin-inactivation on permeability induction in EAE is most likely
539 based on the reduced levels of pro-inflammatory cytokines, which is caused by the reduced numbers of
540 inflammatory leukocytes in the CNS.

541 An earlier study reported on the role of cortactin in the arrangement of molecular components
542 of endothelial junctions. Silencing of cortactin in human brain microvascular endothelial cell cultures
543 by shRNA caused fragmented staining of claudin-5, occludin and ZO-1 (Stamatovic SM, 2015).
544 Contrary to this study, we did not observe differences in the stainings for occludin, ZO-1 or VE-
545 cadherin between primary brain endothelial cells isolated from cortactin$^{-/-}$ and WT mice. Also, whole
546 mount stainings of vibratome sections of the brain of cortactin$^{-/-}$ and WT mice for claudin-5, VE-

cadherin and ZO-1 showed no differences. Whether this is due to species differences or other reasons is presently unknown.

In summary, we have shown that interference with the expression of cortactin protects from the induction of clinical symptoms of EAE by attenuating the entry of inflammatory leukocytes into the CNS of EAE mice. These results establish cortactin as a potential target for reagents interfering with EAE, a model for multiple sclerosis.

Author contributions

MS designed and performed experiments, analysed data and wrote the manuscript; YL designed and performed experiments and analysed data; DV initiated the project, designed experiments, provided overall supervision, and wrote the manuscript. LS aided in EAE analyses, immunofluorescence analyses of inflammatory cuffs and contributed to the manuscript. KR contributed reagents and edited the manuscript.

Abbreviations

BBB, blood-brain barrier; Cttn, cortactin; CNS, central nervous system; EAE, Experimental autoimmune encephalomyelitis; FACS, fluorescence activated cell sorting; MOG, myelin oligodendrocyte glycoprotein; WT, wild type.

Disclosures

The authors declare no financial conflicts of interest.

571 **References**

572 Alon R, van Buul JD (2017) Leukocyte Breaching of Endothelial Barriers: The Actin Link. Trends
573 Immunol 38:606-615.

574 Baluk P, Bolton P, Hirata A, Thurston G, McDonald DM (1998) Endothelial gaps and adherent
575 leukocytes in allergen-induced early- and late-phase plasma leakage in rat airways. Am J Pathol
576 152:1463-1476.

577 Broermann A, Winderlich M, Block H, Frye M, Rossaint J, Zarbock A, Cagna G, Linnepe R, Schulte
578 D, Nottebaum AF, Vestweber D (2011) Dissociation of VE-PTP from VE-cadherin is required
579 for leukocyte extravasation and for VEGF-induced vascular permeability in vivo. J Exp Med
580 208:2393-2401.

581 Butter C BD, O'Neill JK, Turk JL. (1991) Mononuclear cell trafficking and plasma protein
582 extravasation into the CNS during chronic relapsing experimental allergic encephalomyelitis in
583 Biozzi AB/H mice. J Neurol Sci 104:9-12.

584 Cosen-Binker LI, Kapus A (2006) Cortactin: the gray eminence of the cytoskeleton. Physiology
585 (Bethesda) 21:352-361.

586 Cutler RW LA, Barlow CF. (1967) Brain vascular permeability to I-125 gamma globulin and
587 leukocytes in allergic encephalomyelitis. J Neuropathol Exp Neurol 26:558-571.

588 Dudek SM, Jacobson JR, Chiang ET, Birukov KG, Wang P, Zhan X, Garcia JG (2004) Pulmonary
589 endothelial cell barrier enhancement by sphingosine 1-phosphate: roles for cortactin and myosin
590 light chain kinase. J Biol Chem 279:24692-24700.

591 Durieu-Trautmann O, Chaverot N, Cazaubon S, Strosberg AD, Couraud PO (1994) Intercellular
592 adhesion molecule 1 activation induces tyrosine phosphorylation of the cytoskeleton-associated
593 protein cortactin in brain microvessel endothelial cells. J Biol Chem 269:12536-12540.

594 Fenstermacher J GP, Sposito N, Acuff V, Pettersen S, Gruber K. (1988) Structural and functional
595 variations in capillary systems within the brain. Ann N Y Acad Sci 529:21-30.

García Ponce A CMA, Vargas Robles H, Chánez Paredes S, Nava P, Betanzos A, Zarbock A, Rottner K, Vestweber D, Schnoor M. (2016) Loss of cortactin causes endothelial barrier dysfunction via disturbed adrenomedullin secretion and actomyosin contractility. Sci Rep 6:29003.

Heemskerk N, Schimmel L, Oort C, van Rijssel J, Yin T, Ma B, van Unen J, Pitter B, Huveneers S, Goedhart J, Wu Y, Montanez E, Woddfin A, van Buul JD (2016) F-actin-rich contractile endothelial pores prevent vascular leakage during leukocyte diapedesis through local RhoA signalling. Nat Communic 7:10493.

Jacobson JR, Dudek SM, Singleton PA, Kolosova IA, Verin AD, Garcia JG (2006) Endothelial cell barrier enhancement by ATP is mediated by the small GTPase Rac and cortactin. Am J Physiol Lung Cell Mol Physiol 291:L289-L295.

Larochelle C AJ, Prat A. (2011) How do immune cells overcome the blood-brain barrier in multiple sclerosis? FEBS Lett 585:3770-3780.

Leibowitz S KL (1972) Cerebral vascular permeability and cellular infiltration in experimental allergic encephalomyelitis. Immunolgy 22:859-869.

Li-ChunHsieh K SS, Zeller MW, Pulli B, Ali M, Wang C, Chiou TT, Tsang YM, Lee PS, Stossel TP, Chen JW. (2015) Gelsolin decreases actin toxicity and inflammation in murine multiple sclerosis. J Neuroimmunol 287:36-42.

Lutz SE, Smith JR, Kim DH, Olson CVL, Ellefsen K, Bates JM, Gandhi SP, Agalliu D (2017) Caveolin1 Is Required for Th1 Cell Infiltration, but Not Tight Junction Remodeling, at the Blood-Brain Barrier in Autoimmune Neuroinflammation. Cell Rep 21:2104-2117.

Lyck R, Engelhardt B (2012) Going against the tide—how encephalitogenic T cells breach the blood-brain barrier. J Vasc Res 49:497-509.

Mullins RD HJ, Pollard TD. (1998) The interaction of Arp2/3 complex with actin: nucleation, high affinity pointed end capping, and formation of branching networks of filaments. Proc Natl Acad Sci U S A 95:6181-6186.

Nourshargh S, Alon R (2014) Leukocyte migration into inflamed tissues. Immunity 41:694-707.

622 Ransohoff RM, Engelhardt B (2012) The anatomical and cellular basis of immune surveillance in the
623 central nervous system. Nat Rev Immunol 12:623-635.
624 Ruck T BS, Epping L, Herrmann AM, Meuth SG. (2014) Isolation of primary murine brain
625 microvascular endothelial cells. J Vis Exp 93:6-11.
626 Schnoor M, Stradal TE, Rottner K (2018) Cortactin: Cell Functions of A Multifaceted Actin-Binding
627 Protein. Trends Cell Biol 28:79-98.
628 Schnoor M, Lai FP, Zarbock A, Kläver R, Polaschegg C, Schulte D, Weich HA, Oelkers JM, Rottner
629 K, Vestweber D (2011) Cortactin deficiency is associated with reduced neutrophil recruitment
630 but increased vascular permeability in vivo. J Exp Med 208:1721-1735.
631 Sedlakova R SR, Del Maestro RF. (1999) Ultrastructure of the blood-brain barrier in the rabbit. J
632 Submicrosc Cytol Pathol 31:149-161.
633 Sixt M, Engelhardt B, Pausch F, Hallmann R, Wendler O, Sorokin LM (2001) Endothelial cell laminin
634 isoforms, laminins 8 and 10, play decisive roles in T cell recruitment across the blood-brain
635 barrier in experimental autoimmune encephalomyelitis. J Cell Biol 153:933-946.
636 Sorokin L (2010) The impact of the extracellular matrix on inflammation. Nat Rev Immunol 10:712-
637 723.
638 Stamatovic SM SN, Keep RF, Andjelkovic A. (2015) PDCD10 (CCM3) regulates brain endothelial
639 barrier integrity in cerebral cavernous malformation type 3: role of CCM3-ERK1/2-cortactin
640 cross-talk. Acta Neuropathol 130:731-750.
641 Tilghman RW, Hoover RL (2002) The Src-cortactin pathway is required for clustering of E-selectin
642 and ICAM-1 in endothelial cells. FASEB J 16:1257-1259.
643 Uruno T LJ, Zhang P, Fan Yx, Egile C, Li R, Mueller SC, Zhan X. (2001) Activation of Arp2/3
644 complex-mediated actin polymerization by cortactin. Nat Cell Biol 3:259-266.
645 van Rossum AG S-SE, van Buuren-van Seggelen V, Kluin PM, Schuuring E. (2005) Comparative
646 genome analysis of cortactin and HS1: the significance of the F-actin binding repeat domain.
647 BCM Genomics 6:15.

Vestweber D (2015) How leukocytes cross the vascular endothelium. Nat Rev Immunol 15:692-704.

Wessel F, Winderlich M, Holm M, Frye M, Rivera-Galdos R, Vockel M, Linnepe R, Ipe U, Stadtmann A, Zarbock A, Nottebaum AF, Vestweber D (2014) Leukocyte extravasation and vascular permeability are each controlled in vivo by a different tyrosine residue of VE-cadherin. Nat Immunol 15:223-230.

Yang L, Kowalski JR, Zhan X, Thomas SM, Luscinskas FW (2006a) Endothelial cell cortactin phosphorylation by Src contributes to polymorphonuclear leukocyte transmigration in vitro. Circ Res 98:394-402.

Yang L, Kowalski JR, Yacono P, Bajmoczi M, Shaw SK, Froio RM, Golan DE, Thomas SM, Luscinskas FW (2006b) Endothelial cell cortactin coordinates intercellular adhesion molecule-1 clustering and actin cytoskeleton remodeling during polymorphonuclear leukocyte adhesion and transmigration. J Immunol 177:6440-6449.

663 **Figure legends**

664

665 **Figure 1. Cortactin deficiency reduces the severity of MOG_{35-55}-induced experimental**
666 **autoimmune encephalomyelitis.**

667 **(A)** Clinical score of WT mice compared to $Cttn^{-/-}$ mice over time after MOG_{35-55} immunization. Data
668 are representative of three independent experiments with n = 5, 7, 7 (total n = 19/group) WT and
669 $Cttn^{-/-}$ mice (* $p \leq 0.05$; ** $p \leq 0.01$). **(B)** Maximal clinical score, **: p=0.0069**. (C)** area under the curve
670 (AUC) for each group (**: p=0.0065) and **(D)** day of disease onset averaged over all 19 mice (ns:
671 p=0.5658). **(E)** Numbers and percentages of mice with no, mild, or severe clinical scores in each group.
672 Error bars indicate SEM. * $p \leq 0.05$; ** $p \leq 0.01$; ns: not significant. Statistics was analysed with unpaired
673 two-tailed t-test.

674

675 **Figure 2. $Cttn^{-/-}$ and WT mice show comparable peripheral immune responses.**

676 WT and $Cttn^{-/-}$ mice were sacrificed before EAE onset **(A)** or at peak disease (day 16) **(B)** and the
677 number of $CD45^+CD4^+$ T cells and $CD45^+CD11b^+$ myeloid cells was measured in blood, lymph nodes
678 and spleen by flow cytometry. The graphs depict results from two independent experiments with n = 4
679 and 6 (total n = 10/group) WT mice and $Cttn^{-/-}$ mice **(A)**; and from three independent experiments with
680 n = 6, 3 and 5 (total n = 14/group) WT mice and $Cttn^{-/-}$ mice **(B)**. **(C)** Healthy or EAE WT and $Cttn^{-/-}$
681 mice were sacrificed on post-immunization day 12, splenocytes were isolated and restimulated with
682 different concentrations of MOG_{35-55} peptide for 72 h; cell proliferation was determined by colorimetric
683 BrdU proliferation assay. Graphs depict means ± SEM of three independent experiments with n =
684 2/experiment (total n = 6) healthy WT and $Cttn^{-/-}$ mice and n = 3, 4, 4 (total n = 11/group) WT or n =
685 4/experiment (total n = 12/group) $Cttn^{-/-}$ EAE subjected mice. **(D)** Total RNA from $CD45^+$ cells in the
686 blood, lymph nodes and spleens was isolated and IFNγ and IL-17A expression profiles were
687 determined by quantitative RT-PCR; data were normalized to the expression of GAPDH. Expression
688 levels in WT mice were set as 100%. Graphs depict results from three independent experiments with n
689 = 5/experiment (total n = 15/group) WT mice and $Cttn^{-/-}$ mice. Statistics for **(C)** was analyzed with 2-
690 way ANOVA (MOG concentration, $F_{(3, 123)}=10.80$, $p<0.001$; EAE status and genotype, $F_{(3, 123)}=31.06$,
691 $p<0.001$; interaction, $F_{(9, 123)}=2.266$, $p=0.022$) followed by Tukey test (all comparisons of 5 µg/ml
692 MOG vs other concentrations, ****: $p \leq 0.0001$). Statistics for the rest of the graphs was analyzed with
693 unpaired two-tailed Student's *t*-test (ns: not significant).

Figure 3. Leukocyte infiltration and numbers of inflammatory cuffs are reduced during EAE in the absence of cortactin.

WT or Cttn$^{-/-}$ mice were sacrificed when WT mice reached peak EAE; brains were isolated and cell numbers were determined. The total number of CD45^{high} infiltrated leukocytes in WT brains was gated by flow cytometry and set as 100 % **(A)**. Subsequently, the proportions of CD45^{+}CD4^{+} T cells **(B)** CD45^{+}CD8^{+} T cells **(C)**, CD45^{high}CD11b^{+} macrophages **(D),** CD45^{+}Ly6G^{+} neutrophils **(E)** and CD45^{low}CD11b^{+} microglia **(F)** were determined: graphs show proportions of total CD45^{+} leukocytes, CD45^{+}CD4^{+} T cells and CD45^{high}CD11b^{+} macrophages and are means ± SEM of three independent experiments with n=2, 2, 4 (total n=8/group) healthy WT and Cttn$^{-/-}$ mice; n=3, 4, 5 (total n=12) EAE WT mice and n=3, 4, 4 (total n=11) EAE Cttn$^{-/-}$ mice. The graphs shown for CD45^{+}CD8^{+} T cells and CD45^{+}Ly6G^{+} neutrophils are means ± SEM of two independent experiments with n=3 healthy WT and Cttn$^{-/-}$ mice; n=4/experiment (total n=8/group) EAE WT and EAE Cttn$^{-/-}$ mice. **(G-I)** As for **A-F** except that spinal cords instead of brains were analyzed. Results in **(G)** are from three independent experiments with n=4, 5, 6 (total n=15) EAE WT mice and n=4, 4, 6 (total n=14) EAE Cttn$^{-/-}$ mice. Results for **H** and **I** are from three independent experiments with n=2 mice/experiment (total n=6/group) healthy WT and Cttn$^{-/-}$ mice; n=4, 5, 6 (total n=15) EAE WT mice and n=4, 4, 6 (total n=14) EAE Cttn$^{-/-}$ mice. **(J-L)** Leukocytes were isolated from **(J)** brains, **(K)** spinal cords and **(L)** spleens of WT or Cttn$^{-/-}$ mice at the peak of EAE and assessed for CD4^{+} T-bet^{+} IFN-γ^{+} Th1 and CD4^{+} RORγt^{+} IL-17A^{+} Th17 cells populations. Cell numbers were counted by FACS. Results shown for brain and spinal cord are from 2 independent experiments with n=4, 5 (total n=9/group) WT and Cttn$^{-/-}$ mice; results shown for spleen are from 2 independent experiments with n=4, 5 (total n=9) WT and n=4 each (total n=8) Cttn$^{-/-}$ mice. **(O)** Cryo-sections of brains isolated from mice treated as above (isolated at peak stage of EAE in WT mice) were stained with anti-CD45 for leukocytes (magenta) and with pan-laminin antibodies (green) for identification of perivascular cuffs. Bar=100µm. **(N)** The number of perivascular cuffs in four distinct sections per mouse was counted in three independent experiments with n=5, 5 and 6 WT mice and Cttn$^{-/-}$ mice (total n=16/group). **(O)** Average size of inflammatory cuffs was measured in 10 WT (71 cuffs in total) and 5 Cttn$^{-/-}$ mice (41 cuffs in total). Statistics: Unpaired two-tailed Student's *t*-test was used for **(A)** *: p=0.0174, **(G)** *: p=0.0273, **(K)** **: p=0.012, **(O)** p=0.44). **(N)** Mann Whitney U-test, *: p=0.0158. **(B)** 2-way ANOVA (healthy/EAE, $F_{(1,34)}$=33.71, p<0.0001; genotype, $F_{(1,34)}$=4.126, p=0.0501; interaction $F_{(1,34)}$=3.398, p=0.074) followed by Tukey test: EAE WT vs EAE KO *: p=0.0114; healthy WT vs EAE WT ****: p≤0.0001. **(C)** 2-way ANOVA (healthy/EAE, $F_{(1,17)}$=6.729, p=0.0189; genotype, $F_{(1,17)}$=2.378, p=0.14415; interaction

$F_{(1,17)}$=1.862, p=0.1902) followed by Tukey test: healthy WT vs EAE WT *: p=0.03, EAE WT vs EAE KO *: p=0.04. **(D)** 2-way ANOVA (health/EAE, $F_{(1,35)}$=41.39, p<0.0001; genotype, $F_{(1,35)}$=2.936, p=0.0955; interaction $F_{(1,35)}$=1.912, p=0.1755) followed by Tukey test: healthy KO vs EAE KO **: p=0.0061; healthy WT vs EAE WT ****: p≤0.0001. **(E)** 2-way ANOVA (interaction $F_{(1,17)}$=3.898, p=0.0648; healthy/EAE, $F_{(1,17)}$=15.07, p=0.0012; genotype, $F_{(1,17)}$=0.9879, p=0.3342) followed by Tukey *post hoc* test: EAE WT vs EAE KO *: p=0.0306; healthy WT vs EAE WT **: p=0.0016. **(F)** 2-way ANOVA (healthy/EAE, $F_{(1,35)}$=0.1962, p=0.6605; genotype, $F_{(1,35)}$=0.9648, p=0.3327; interaction $F_{(1,35)}$=0.3970, p=0.5327) followed by Tukey test: healthy WT vs EAE WT p=0.4490, EAE WT vs EAE KO p=0.2167. **(H)** 2-way ANOVA (health/EAE, $F_{(1,37)}$=15.18, p=0.0004; genotype, $F_{(1,37)}$=2.613, p=0.1145; interaction $F_{(1,37)}$=2.666, p=0.1110) followed by Tukey test: EAE WT vs EAE KO *: p=0.0237, healthy WT vs EAE WT **: p=0.002). **(I)** 2-way ANOVA (health/EAE, $F_{(1,37)}$=9.911, p=0.0032; genotype, $F_{(1,37)}$=2.244, p=0.1426; interaction $F_{(1,37)}$=1.210, p=0.2783) followed by Tukey test: EAE WT vs EAE KO *: p=0.0267, healthy WT vs EAE WT *: p=0.0227). All graphs show mean ± SEM.

Figure 4. Leukocyte infiltration and demyelination in the spinal cord is reduced in cortactin-deficient mice during EAE.

WT or $Cttn^{-/-}$ mice were sacrificed when WT mice reached peak EAE. The lumbar parts of the spinal cords were isolated, sectioned and examined for inflammatory foci and for axonal demyelination by H&E and LFB staining, respectively. **(A)** Representative staining of inflammatory foci (inserts show higher magnifications of marked areas) and demyelination (arrowheads point at areas of demyelination). **(B)** Quantification of the number of inflammatory foci (with WT mice at peak EAE set as 100%) in 4 random sections per mouse. The graph shows means ± SEM of three independent experiments with n=4, 5, 6 WT mice (total n=15) and n=4/experiment (total n=12) $Cttn^{-/-}$ mice (***: p=0.0002). **(C)** The area of demyelination in 3 random sections/mouse. The graph shows means ± SEM of four independent experiments with n=4, 4, 6, 6 (total n=20) WT mice and n=4, 4, 5, 6 (total n=19) $Cttn^{-/-}$ mice (***: p=0.0001). Scale bar=150 μm. Statistics was analysed with unpaired two-tailed Student's *t*-test.

Figure 5. Lack of cortactin leads to lower levels of proinflammatory cytokines in the inflamed CNS.

WT or $Cttn^{-/-}$ mice were sacrificed at peak EAE and total RNA from brains and spinal cords were isolated. Cytokine expression in brain **(A)** and spinal cord **(B)** was measured by quantitative RT-PCR. mRNA expression was normalized to GAPDH and gene expression in WT mice was set as 100%.

761 Graphs depict means ± SEM of three independent experiments with n=3, 5, 6 (total n=14) for EAE WT
762 mice and EAE Cttn$^{-/-}$ mice. Statistics was analysed with unpaired two-tailed Student's *t*-test (brain:
763 IFNγ, TNF-α, IL-6, MCP-1, CCR2; spinal cord: TNF-α, IL-6, MCP-1, RANTES, IL-17), or with Mann
764 Whitney U-test (brain: IL-1, RANTES, IL-17, CXCL1; spinal cord: IFNγ, IL-1, CCR2, CXCL1).
765 Brain, *: p=0.0251 (CCR2), *: p=0.0165 (TNF-α), ***: p=0.0003 (RANTES). Spinal cord, *:
766 p=0.0138 (CXCL1), **: p=0.002 (IL-1β), **: p=0.005 (IL-6, MCP-1), ***: p=0.0006 (IFNγ), ***:
767 p=0.0002 (CCR2), ****=p≤ 0.0001 (TNF-α, RANTES).

768 **Figure 6. Lack of cortactin results in reduced vascular permeability in the inflamed CNS.**

769 Healthy and EAE-subjected WT or Cttn$^{-/-}$ mice were injected i.v. with Evans blue on day 10 p.i. and
770 sacrificed 24h later. Animals were perfused with PBS and brains **(A)**, spinal cords **(B)** and kidneys **(C)**
771 were isolated. The dye was extracted from tissue and measured at 620 nm; data are expressed relative
772 to organ weight. Graphs depict mean ± SEM of three independent experiments with n=3, 5 (total
773 n=8/group) for healthy WT or Cttn$^{-/-}$ mice; n=5, 6, 6 (total n=17) for EAE subjected WT mice and
774 with n=4, 6, 6 (total n=16) for EAE subjected Cttn$^{-/-}$ mice. **(D, E)** Similar to **(A, B)** except that brain
775 and spinal cord permeability was measured on the peak of EAE (d17 p.i.) and animals were sacrificed
776 1h after Evans blue injections. The graphs shown are mean ± SEM of experiment with n=4/group for
777 WT or Cttn$^{-/-}$ mice. **(F)** Representative cryosections of brains from WT mice and Cttn$^{-/-}$ mice on the
778 peak of EAE, stained with anti-pan-laminin antibodies. Bar=100 µm. **(G)** Average vessel density was
779 measured in 5 different areas/animal with n=5 mice/group for WT and Cttn$^{-/-}$. Statistics was analysed
780 with: **(A)** 2-way ANOVA (healthy/EAE, $F_{(1,44)}$=8.324, p=0.006; genotype, $F_{(1,44)}$=3.704, p=0.0608;
781 interaction $F_{(1,44)}$=7.274, p=0.0099) followed by Tukey test: EAE WT vs EAE KO **: p=0.0014,
782 healthy WT vs EAE wt **: p=0.002. **(B)** 2-way ANOVA (healthy/EAE, $F_{(1,44)}$=15.60, p=0.0003;
783 genotype, $F_{(1,44)}$=4.006, p=0.0515; interaction $F_{(1,44)}$=7.648, p=0.0083) followed by Tukey test: healthy
784 WT vs healthy KO **: p=0.002, healthy WT vs EAE WT ***: p=0.0001, EAE WT vs EAE KO ***:
785 p=0.0009. **(C)** 2-way ANOVA (healthy/EAE, $F_{(1,44)}$=19.14, p<0.0001; genotype, $F_{(1,44)}$=0.1582,
786 p=0.6927; interaction $F_{(1,44)}$=0.4692, p=0.4969) followed by Tukey test: healthy WT vs EAE WT *:
787 p=0.00382, healthy KO vs EAE KO **: p=0.0074. Statistics for **(D)**, **(E)**, **(G)** was analysed with
788 unpaired two-tailed Student's *t*-test: **(D)** p=0.3244, **(E)** p=0.097**, (G)** p=0.12. The graph shows mean ±
789 SEM.

790

791 **Figure 7. Cortactin expression in primary mouse brain microvascular endothelial cells**
792 Immunofluorescence staining of cultured MBMEC, isolated from the brains of five WT and Cttn$^{-/-}$
793 mice. Staining was performed with antibodies against cortactin and VE-cadherin and with Hoechst to

detect cell nuclei. Primary antibodies were detected with Alexa 488-, and Alexa 647-conjugated secondary antibodies and visualized by fluorescence microscopy. Scale bar=50 μm.

Figure 8. Protein expression of adhesion and tight junction proteins in the brain vasculature of Cttn$^{-/-}$ and WT mice.

(A) Immunofluorescence staining of MBMEC, isolated from the brains of 5 WT and Cttn$^{-/-}$ mice, for occludin, VE-cadherin and ZO-1. **(B)** Whole mount staining of blood vessels in vibratome sections from healthy WT and Cttn$^{-/-}$ brains for claudin-5, VE-cadherin and ZO-1 (inserts show higher magnification) Scale bar=50 μm. Images are representative for at least three independent preparations each. Mean fluorescence intensity of the staining for junctional proteins in brain sections was quantified for claudin-5 **(C)**, VE-cadherin **(D)** and ZO-1 **(E)**. The graphs shown are mean ± SEM with n=8 WT and n=10 Cttn$^{-/-}$ mice **(C)**; n=6 WT and n=8 Cttn$^{-/-}$ mice **(D)**; n=8 WT and n=6 Cttn$^{-/-}$ mice **(E)**. Statistics for was analysed with **(C)** Mann Whitney U-test p=0.3599; unpaired two-tailed Student's *t*-test: **(D)** p=0.4893, **(E)** p=0.9694.

Figure 9. RNA expression of junctional molecules in healthy and inflamed CNS of Cttn$^{-/-}$ and WT mice.

Total mRNA was isolated from Cttn$^{-/-}$ and WT mice at the peak of EAE **(A, B)** and without EAE **(C, D)** and gene expression was measured by means of qRT-PCR (normalized to GAPDH expression) with expression levels in WT mice set as 100%. The graphs shown are mean ± SEM of three independent experiments with n=3, 5, 6 (total n=14) for EAE subjected WT mice and Cttn$^{-/-}$ mice; and two independent experiments n=2, 2 (total n=4/group) for healthy WT and Cttn$^{-/-}$ mice. Statistics was analysed with unpaired two-tailed Student's *t*-test: **: p=0.002 (occludin) **: p=0.005 (VE-cadherin).

Figure 10. Lack of cortactin impairs T cell transmigration through primary brain endothelial cells.

Assays were performed with MBMEC isolated from WT and Cttn$^{-/-}$ mice. **(A)** Transmigration of murine OTII-OVA CD4^{+} T cells across a TNF-α activated monolayer of MBMEC on transwell filters (3 μm pore size) in the presence of 100 ng/ml SDF-1 for 1h and 3.5h (as indicated). The number of transmigrated cells is displayed as percentage of total applied cells. The graphs shown are mean ±SEM

of three independent experiments with n=6, 6, 7 (total n=19) filters for WT; n=6, 6, 8 (total of n=20) filters for Cttn$^{-/-}$ cells. **(B)** T cells (as above) were allowed to bind to EC (as above) in a 96-well plate for 30 min. The number of adherent cells to WT EC was set as 100%. The graph shows mean ±SEM of two independent experiments with n=8, 10 (total n=18) well for WT and Cttn$^{-/-}$ cells. **(C)** T cells (as above) were passed over EC (as above) under flow conditions increasing from 0 to 2dyn/cm^2 for 30 min in a six-channel μ-Slide VI 0.4 (Ibidi) in the presence of 50 ng/ml SDF-1. The graph shows mean ±SEM of 20 channels for WT and Cttn$^{-/-}$ EC. Statistics for was analysed with unpaired two-tailed Student's *t*-test: **(A)** **: p=0.0015, ***: p=0.0003, **(B)** p=0.9293, **(C)** p=0.2324.

Figure 11. ICAM-1 expression in primary brain endothelial cells after TNFα is not affected by cortactin deficiency

(A) A representative immunofluorescence staining of MBMEC of indicated genotypes stimulated or unstimulated for 8h with TNFα. Staining was performed with antibodies against ICAM-1 and VE-Cad. Scale bar=50 μm. **(B)** Quantification of ICAM-1 expression per unit area was performed with ImageJ. Shown are means ± SEM of 16 (unstimulated) or 32 (stimulated) measurement areas (0.01 mm^2) per genotype. ns, not significant, ****p<=0.001, Kruskal-Wallis 1-way Analysis of Variance on Ranks was performed (H=60.061, df=3) followed by Dunn's test.

Figure 1

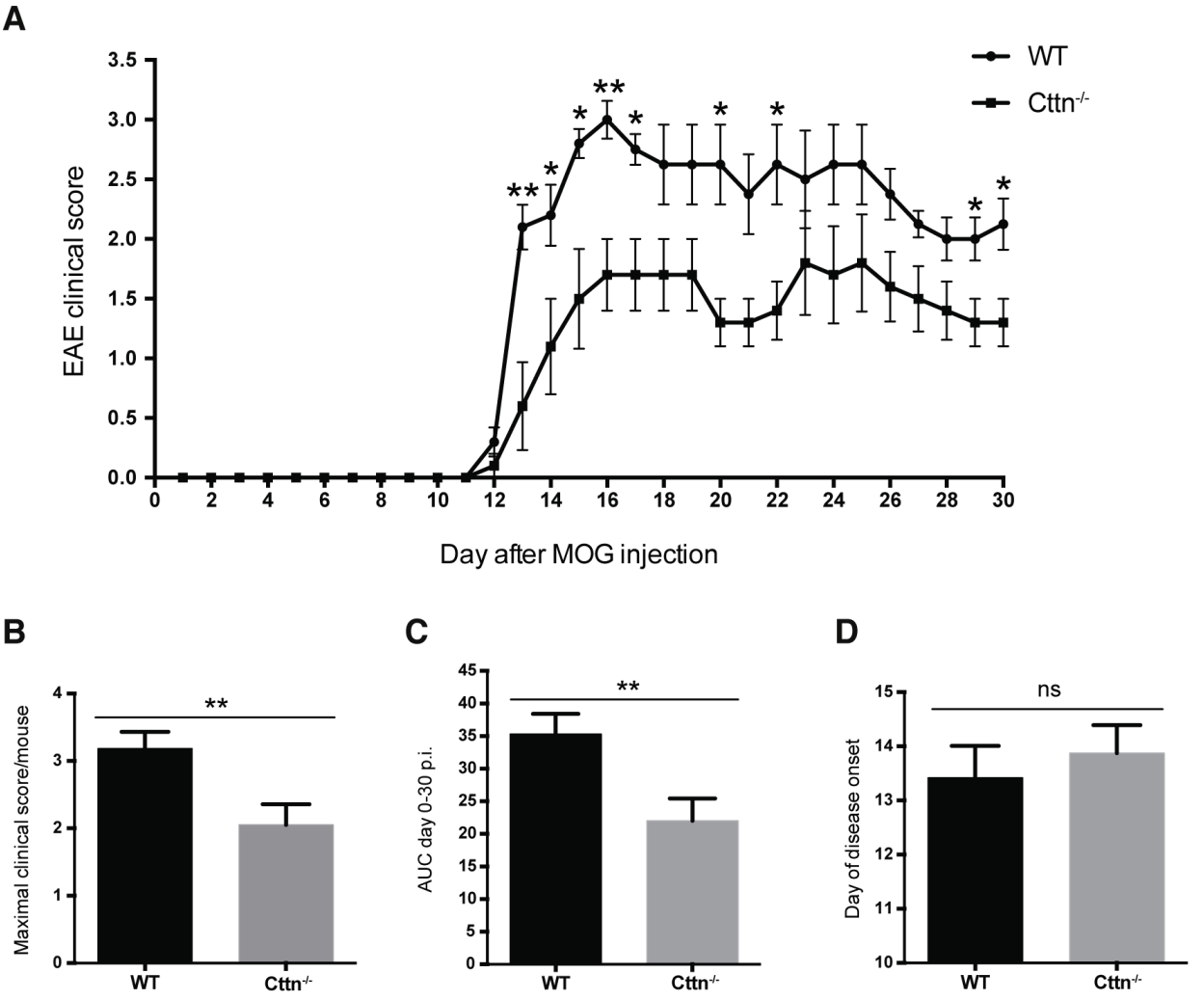

E

	No clinical score (% [n])	Mild clinical score 1-2 (% [n])	Severe clinical score 3-5 (% [n])
WT	0 (0/19)	15,8 (3/19)	84,2 (16/19)
Cttn$^{-/-}$	15,8 (3/19)	57,9 (11/19)	26,3 (5/19)

Figure 2

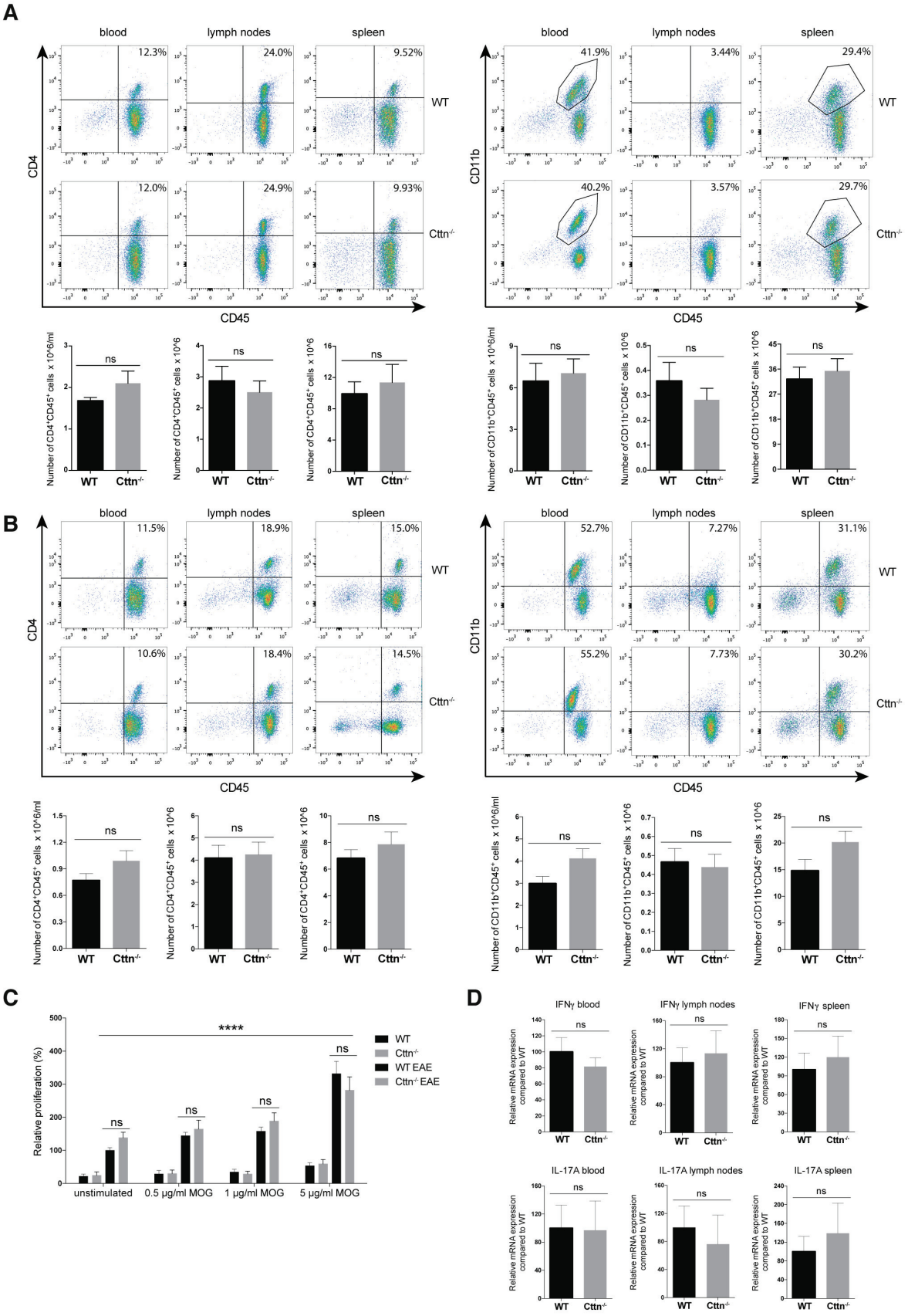

Figure 3

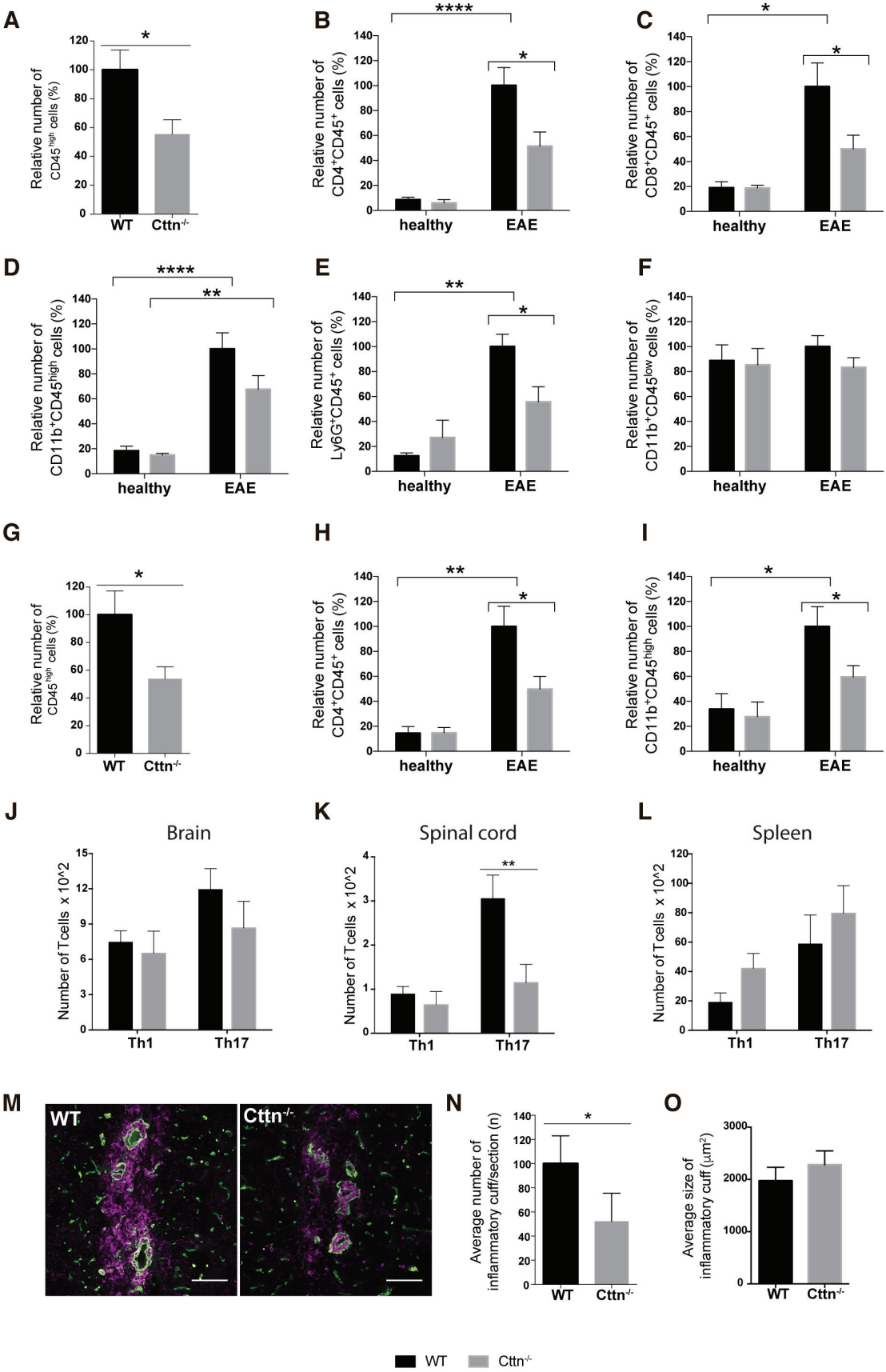

Figure 4

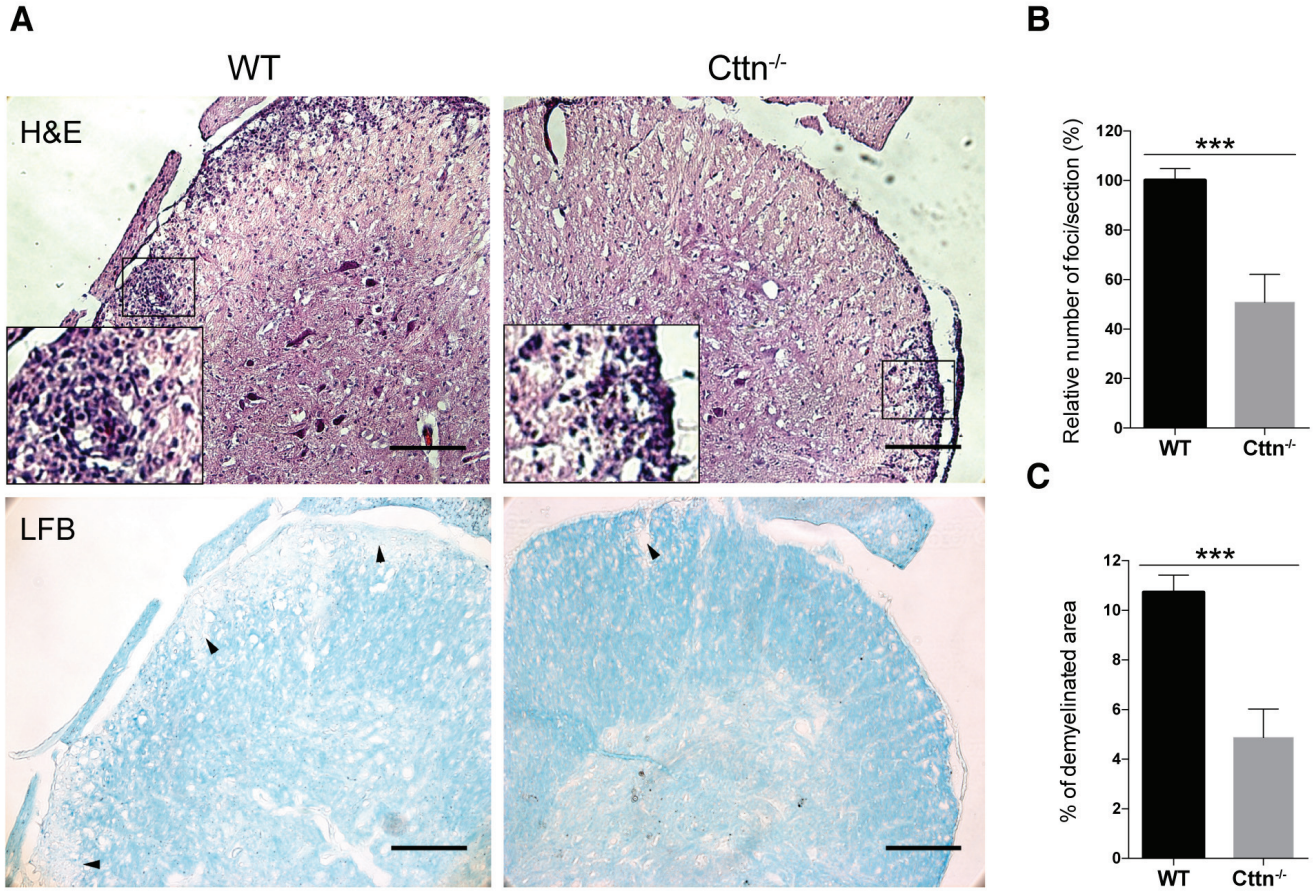

Figure 5

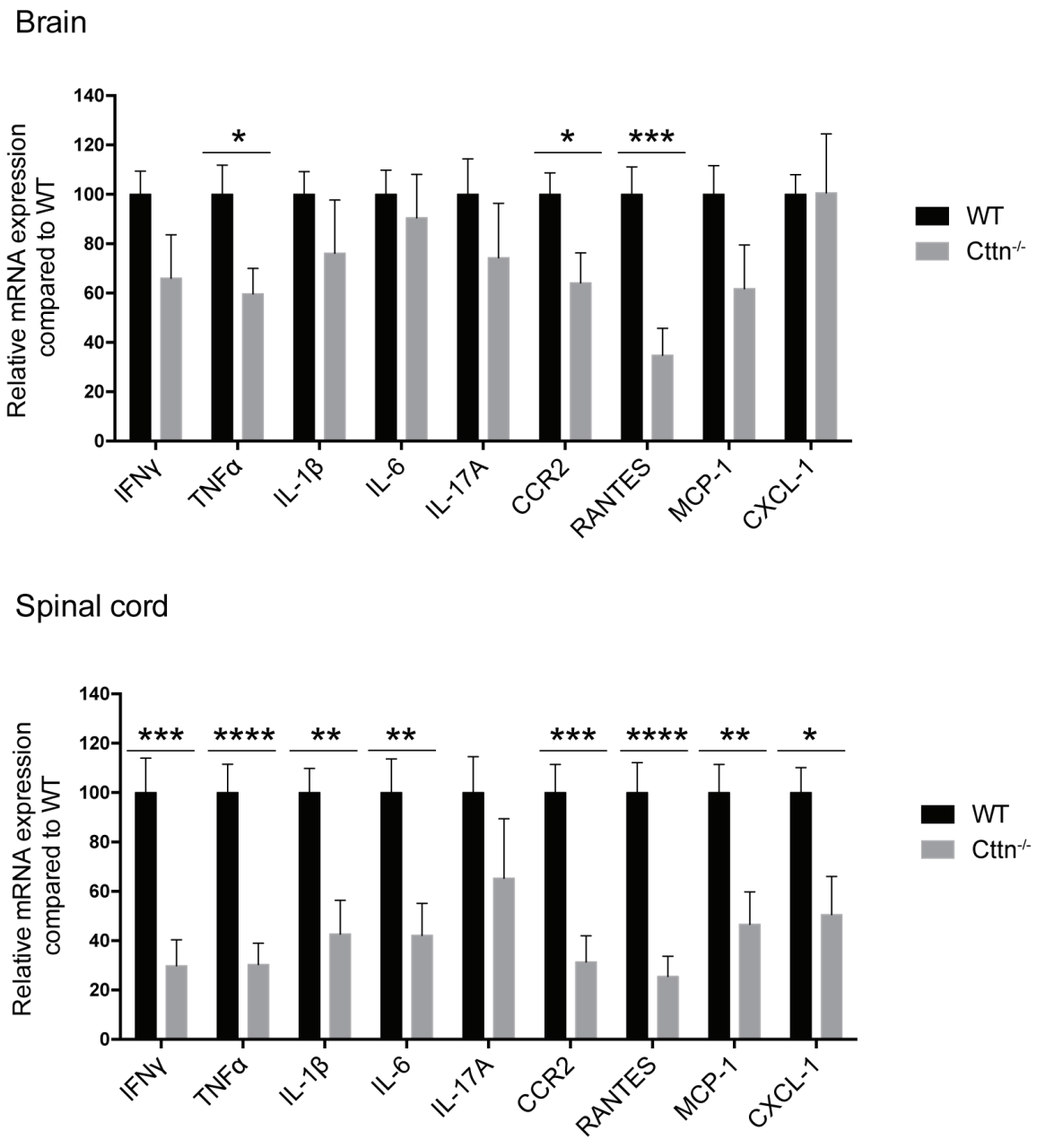

Figure 6

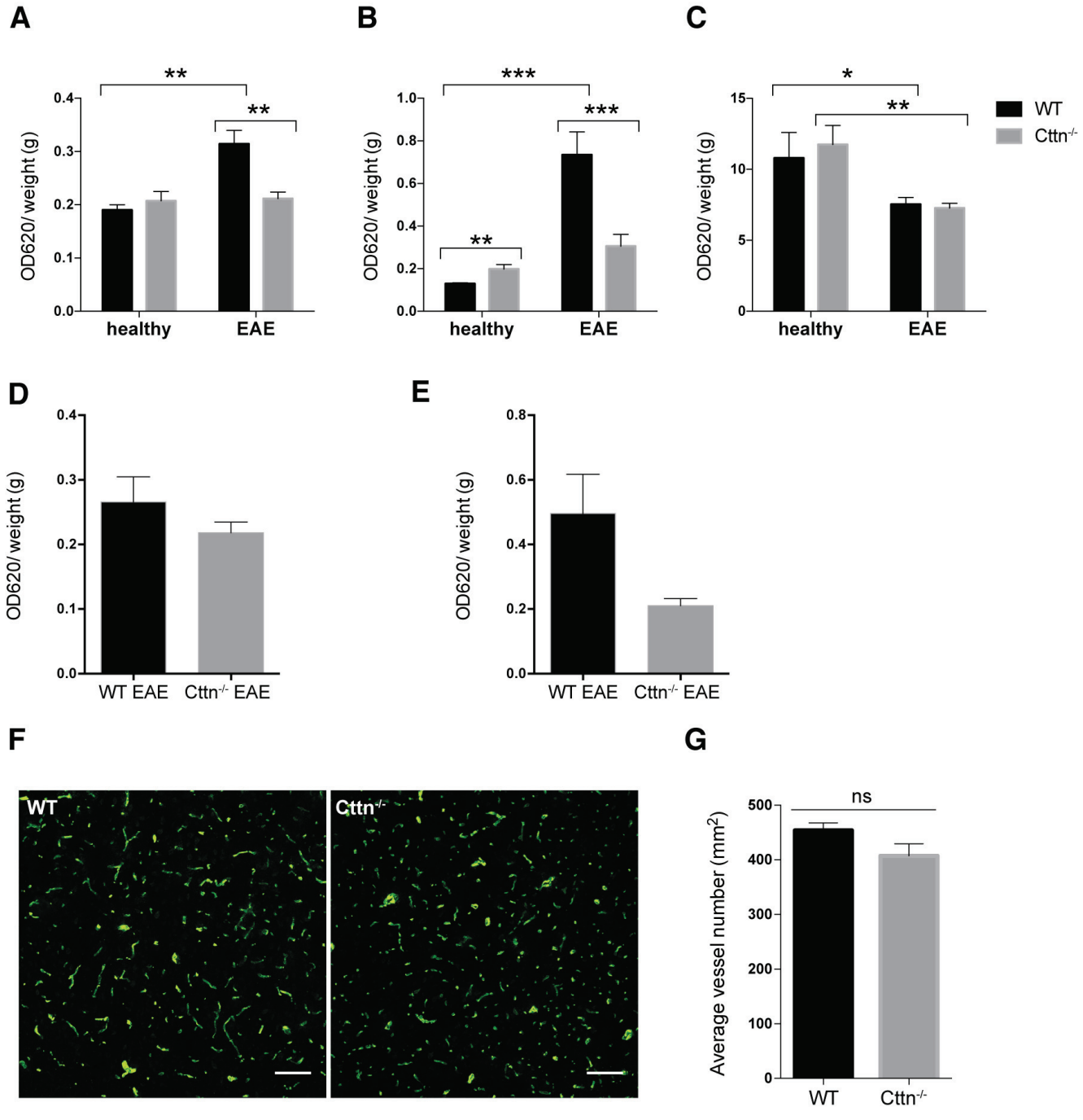

Figure 7

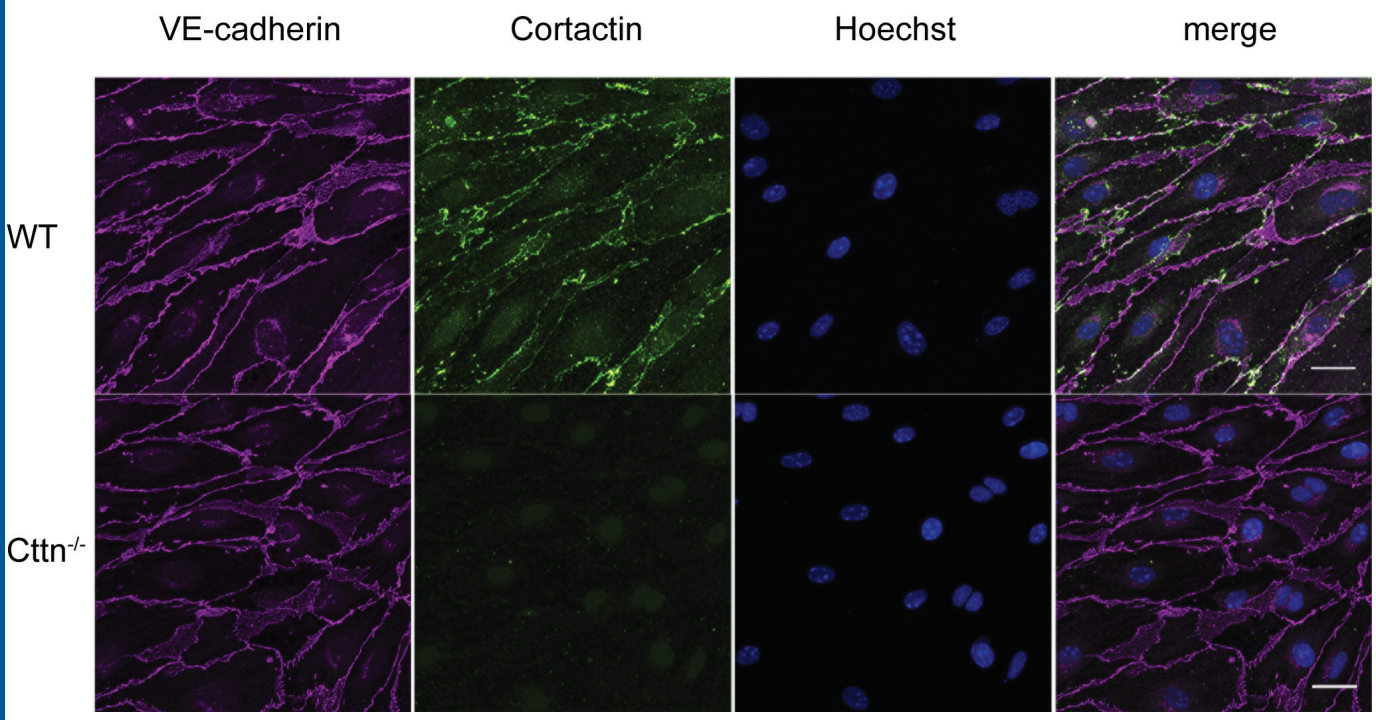

Figure 8

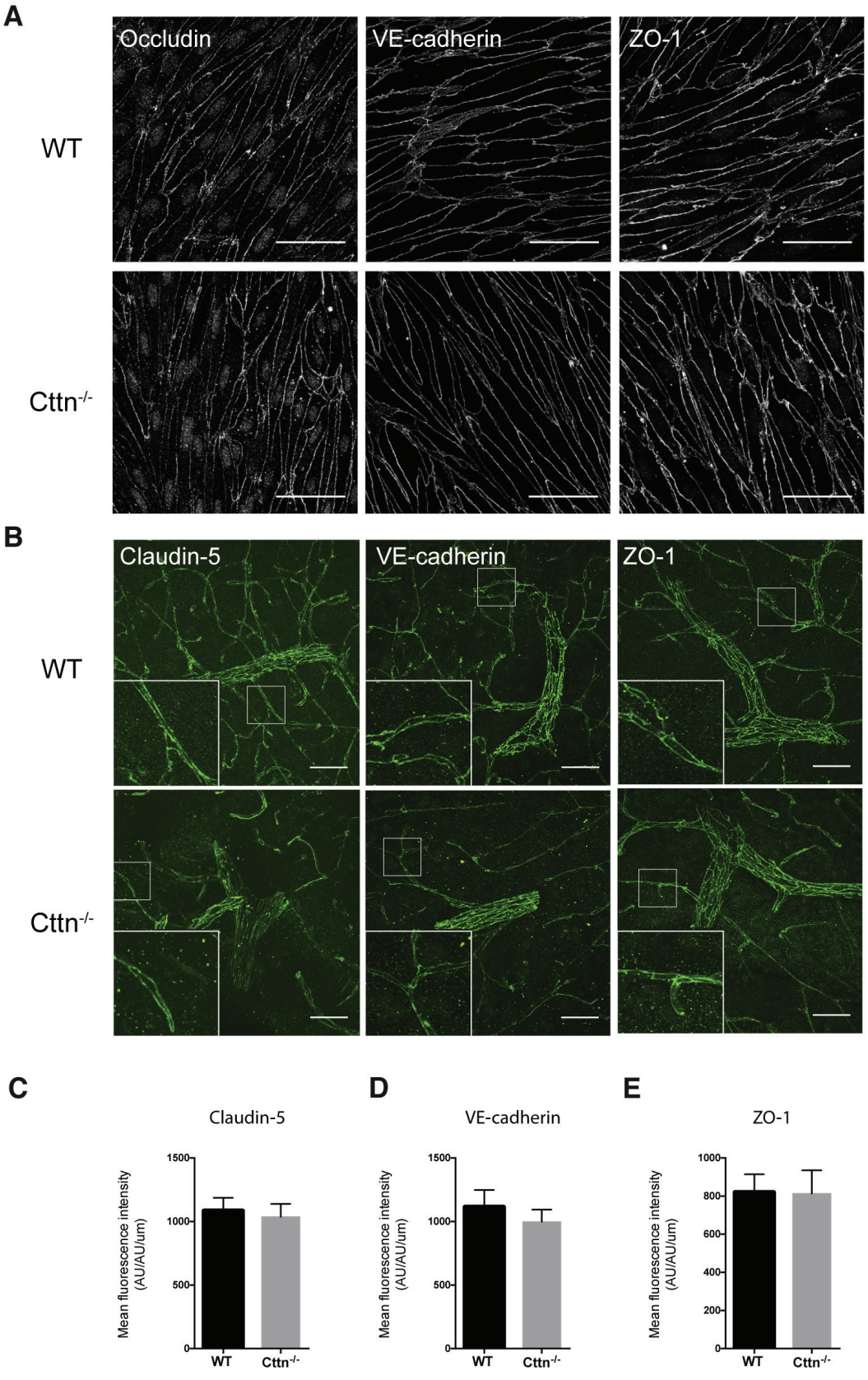

Figure 9

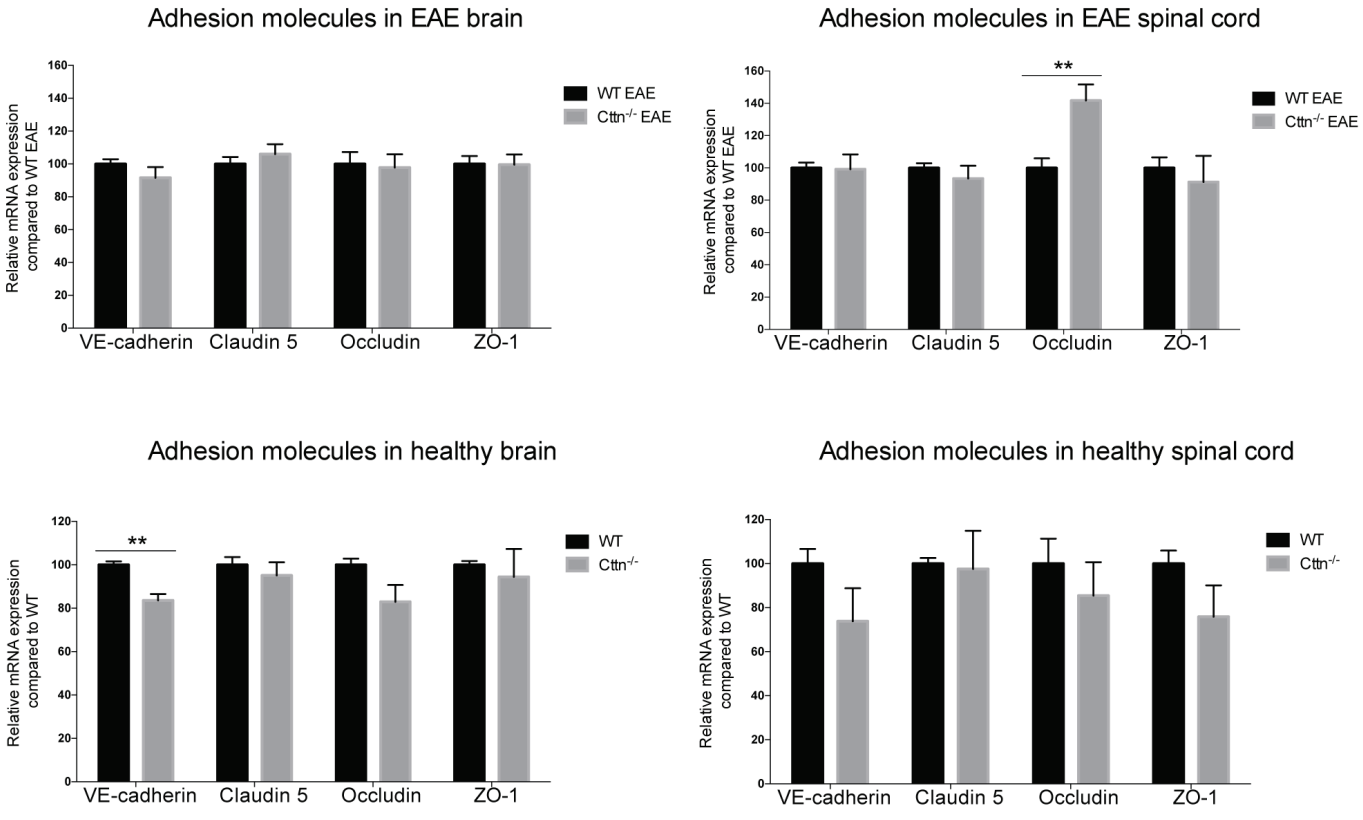

Figure 10

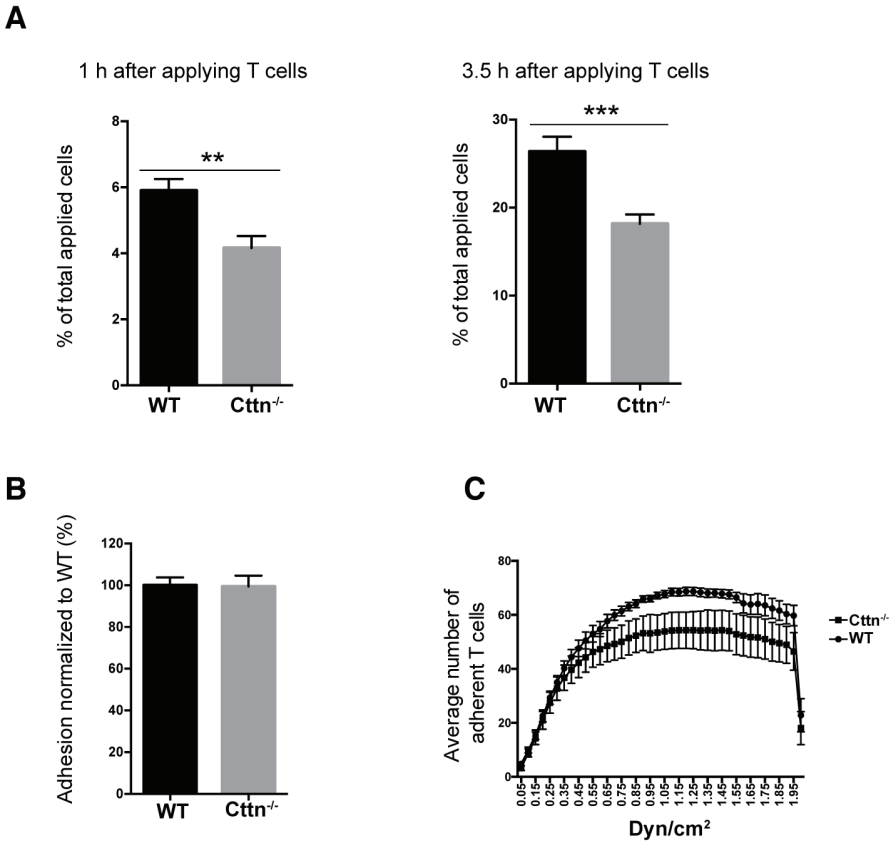

Figure 11

A

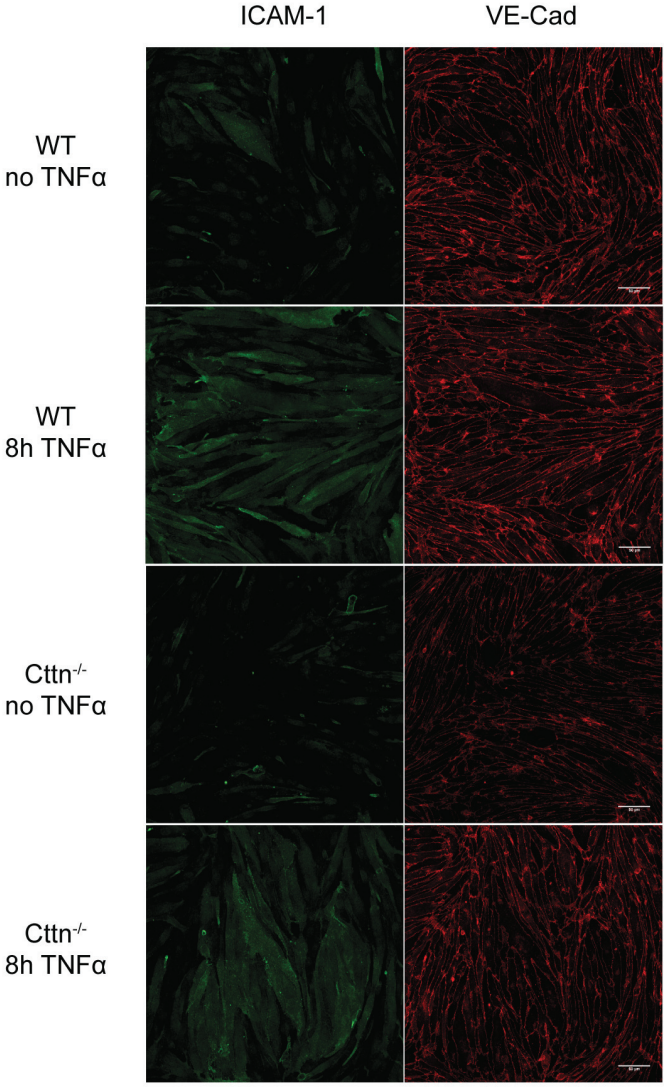

B